

MODELLED RESPONSE OF EXTRATROPICAL CYCLONE
CASES IN THE GREAT PLAINS TO PROJECTED LATE
TWENTY-FIRST CENTURY SNOW COVER EXTENTS

by

Ryan Clare

A thesis submitted in partial fulfillment of
the requirements for the degree of

Master of Science

(Atmospheric and Oceanic Sciences)

at the

UNIVERSITY OF WISCONSIN-MADISON

2018

Abstract

The North American Great Plains region has high snow cover variability and high maximum snow albedo, especially relative to its background surface albedo. The region is adjacent to two major storm tracks consequential to weather in the Midwest, Great Lakes region, and Northeast. The relationship between snow cover in the region, extratropical cyclone trajectories, and a changing climate is explored.

Large ensemble simulations with the Weather Research and Forecasting model (WRF) were forced with projected late twenty-first century extents of snow from models of the CMIP5 project to test the effects on extratropical cyclones contributed solely by the snow cover of a changing climate. The experiment induces an adjustment to the extent of snow cover in North America according to tenth, fiftieth, and ninetieth percentile reductions in winter and spring snow cover for the late twenty-first century (2080-2099) in the RCP4.5 and RCP8.5 experiments initialized zero to four days prior to cyclogenesis. The effects on 15 individual extratropical cyclone cases across 375 distinct simulations are analyzed.

There is a strong tendency for more intense storms to adhere more closely to the southern extent of snow. Snow cover reductions directly induce the strengthening of extratropical cyclones and cause them to deviate from their original trajectory while increasing the total amount of precipitation and reducing the amount of that precipitation which falls as snow. All of these are associated with the amount of snow removed but their specific relationship to the margin of snow extent is tenuous. Responses to snow removal are weakest in November and December and greatest in March.

Table of Contents

0 Foreword	vi
0.1 Acknowledgements	vii
1 Introduction	1
1.1 Physical Effects of Snow Cover	1
1.1.1 Albedo.....	1
1.1.2 Temperature	3
1.1.3 Atmospheric Moisture	5
1.2 Snow Cover Trends.....	6
1.2.1 Historical and Present.....	6
1.2.2 Projected.....	7
1.3 Extratropical Cyclones	8
1.3.1 Projected Trends	9
1.4 Cyclones and Snow Cover	10
1.5 Motivation for this Study	12
2 Data and Methods	14
2.1 Domain	14
2.2 Case Selection	15
2.3 Data	16
2.3.1 North American Regional Reanalysis (NARR).....	16
2.3.2 CMIP5	17
2.4 Model Physics	18
2.4.1 Noah Land Surface Model.....	19
2.5 Experimental Design	22
2.5.1 Snow line determination.....	22
2.5.2 Snow removal	24
2.5.3 WRF simulations	25
2.5.4 Cyclone tracking.....	26
3 Results	27
3.1 Snow cover trends	27

3.2 Pressure changes	28
3.3 Trajectory departures.....	29
3.4 Precipitation changes.....	31
3.5 Snow line adherence.....	32
3.6 Changes for cities	33
4 Discussion.....	34
5 Conclusion	38
6 References.....	40
7 Figures and Tables.....	49

List of Figures and Tables

Figure 1: From Brutel-Vuilmet et al. (2013), the relative snow cover extent decrease in the twenty-first century as a function of representative concentration pathway	50
Figure 2: North American maximum snow albedo and background surface albedo difference	51
Figure 3: Study domain with grid.....	52
Figure 4: Cyclone trajectories for the 15 cases used in this study	53
Table 1: CMIP5 models used in this study and their attributes	54
Figure 5: Fractional decrease in snow albedo by age for accumulating and ablating snow fields.....	55
Figure 6: CMIP5 model snow retreat values for late twentieth to late twenty-first centuries by month with 10%, 50%, and 90% values marked.....	56
Table 2: Models used for each month's 10%, 50%, and 90% snow retreat values	57
Figure 7: Observed and applied snow extents for 10% snow retreats for all cases.....	58
Figure 8: As for Figure 7 but for median snow retreat values.....	59
Figure 9: As for Figures 7 and 8 but for ninetieth percentile snow retreat values.....	60
Figure 10: Histogram of mean pressure change for all simulations	61
Figure 11: As for Figure 10 but for maximum pressure decrease	62
Table 3: Percentage of simulations with mean pressure decreases by snow removal amount and initialization time	63
Figure 12: Maximum pressure decrease across all simulations by cold season period....	64
Figure 13: Histogram of mean trajectory deviation for all simulations.....	65
Figure 14: Relation between mean trajectory deviation and snow removal amount.....	66
Table 4: Average mean trajectory deviation categorized by snow removal amount and initialization time	67
Figure 15: Mean trajectory deviation across all simulations by cold season period	68
Figure 16: Relationship between observed minimum central SLP and snow line adherence	69
Figure 17: Cities examined in this study	70

Table 5: Minimum, average, and maximum temperature differences in each city for the January-February period	71
---	----

0 Foreword

“The climate is changing: we have a new normal. The environment in which all weather events occur is not what it used to be. All storms, without exception, are different. Even if most of them look just like the ones we used to have, they are not the same.”

-Trenberth et al., 2015

0.1 Acknowledgements

Support for this project was provided in its first year by the University of Wisconsin Graduate School and, since then, by the National Science Foundation (NSF AGS-1640452). Specialized computing resources have been provided by the University of Wisconsin Center for High Throughput Computing.

The debt of gratitude which I owe to my advisor Ankur Desai cannot be overstated. His wisdom, patience, and positivity have made this all possible. I would like to thank Drs. Jon Martin, Michael Notaro, and Steve Vavrus who, as members of my research team and advisory committee, have provided much of their time and invaluable guidance. I would also like to thank my undergraduate advisor, Shane Mayor, who provided me with the direction and inspiration to get this far.

I would like to thank my parents who have given me every opportunity to succeed and supported me every step of the way. I would be remiss not to profusely thank Hannah, who has been with me since this began and done everything she could to pick up slack and help me while I've been distracted and busy.

And of course, none of this would have even been thinkable without the generosity of strangers. The patient professionals of the National Center for Atmospheric Research which respond to queries made to wrfhelp and on the ncl-talk forum have been instrumental to this project. The countless brilliant individuals who have provided their wealth of knowledge for free on websites like Stack Exchange will forever have my gratitude and I hope that someday, I will be able to give back in my own way.

Honorable mentions: Nicholas Nelson, Molly, Ammara, Ke, James, Toma, & Jackson (the dog)

1 Introduction

1.1 Physical Effects of Snow Cover

Snow cover is a seasonal phenomenon which contributes to a wide range of effects on the overlying atmosphere both near and far. On average, the maximum snow extent in the Northern Hemisphere reaches nearly $45 \times 10^6 \text{ km}^2$ in January (Robinson and Dewey, 1990; Lemke et al., 2007), covering over 50% of the land in the extratropics (Robinson and Frei, 2000) and making Northern Hemisphere snow cover the largest component of the terrestrial cryosphere. Properly understanding the extent and depth of snow throughout the globe and the impacts that those factors contribute is of incredible importance to making more accurate forecasts. As a boundary forcing, snow plays a critical role in influencing inter- and intra-annual variability in middle-latitude atmospheric circulation (Shukla, 1984). Jeong et al. (2013) found that by initializing climate model hindcasts with observed snow data, potential predictability of surface air temperatures increased substantially up to 2 months out. The general properties of snow are universal but their net effects are highly dependent on geographical, micrometeorological, and other local conditions.

1.1.1 *Albedo*

Albedo is a quantification of shortwave reflectivity measured between values of 0 and 1. This expresses the proportion of incident solar radiation reflected by a surface as a fraction of the total amount of incoming solar radiation. The complement of shortwave reflectivity is shortwave absorptivity. On land surfaces, incoming shortwave radiation which is not reflected is absorbed where it usually has an immediate heating effect (Petty, 2006).

Snow, as it is mostly white, is highly reflective in the visible portion of the electromagnetic spectrum. The increase in outgoing shortwave radiation is proportional to the increase in albedo of snow-covered land (Baker et al., 1992). Bauer and Dutton (1962), using aircraft observations, stated that albedo essentially has two seasonal values determined by the presence or absence of snow. This is not an entirely satisfactory framework as snow in any given location is subject to sizeable variations in albedo due to the snow's age (Livneh et al., 2010), depth (up to 5 inches; Kung et al. 1964), grain size (Marshall and Oglesby, 1994), and the presence of impurities (Warren, 1984) but even snow with relatively low albedo is almost always more reflective than bare ground (snow may have lower albedo than otherwise bright surfaces such as that of the Bonneville Salt Flats in Utah; Eaton and Dirmhirn, 1979). The effectiveness of a snow field's albedo is determined by the local vegetation, surface roughness, solar angle, and cloud cover to name just a few factors (Kung et al., 1964; Carroll and Fitch, 1981).

On a clear day, the albedo of fresh snow can exceed 0.85 (Zhang, 2005). The average snow-covered albedo of the North American continent is 0.56, which is roughly 3.5 times greater than when snow is not present (Robinson and Kukla, 1985). The north-south difference in albedo across the boundary of snow-covered ground may be as high as 0.67 while that same difference only reaches 0.03 in the summer when no snow is present (Kung et al., 1964). The local maximum of snow albedo in North America is highest in the Great Plains region where the surface is relatively flat and free of forests (Robinson and Kukla, 1985). Typically, the albedo of fresh snow in autumn and early winter is much greater than that of the wet, old snow in spring (Zhang, 2005).

1.1.2 Temperature

Snow albedo and the resultant amount of shortwave radiation reflected from the Earth's surface have a direct impact on the temperature of the overlying atmosphere (Budyko, 1969; Dewey, 1977; Leathers et al., 1995). Daily air temperatures near the surface may be reduced by 5°-10°C by underlying snow cover (Dewey, 1977) and positive temperature departures are actively suppressed in the Great Plains (Robinson and Hughes, 1991) where the correlation between snow cover and negative temperature anomalies is the strongest in North America (Heim and Dewey, 1984). Monthly-averaged temperatures have been shown to be 2°-5°C lower over snow (Wagner, 1973; Namias, 1985) and mean temperatures for entire winters may be 0.5°-2.0°C lower in regions where snow is present (Yershov, 1998; as referenced in Zhang, 2005). Vavrus (2007) determined, through global climate model (GCM) simulations with all terrestrial snow cover eliminated, that snow cover in North America contributed to an average 5°C lower surface air temperature annually. Walland and Simmonds (1997), using the Melbourne University GCM, simulated a Northern Hemisphere with very extensive snow cover and again with a low snow cover extent and found temperature anomalies as great as 6°C at 75 m and consistent temperature responses at 850 hPa with less consistent though some significant responses at 500 hPa. The greatest significant responses were simulated in the Arctic.

The average emissivity of snow is 0.98, higher than that of any other type of land surface, which contributes to considerable outgoing longwave radiation which cools the snow's surface (Zhang, 2005). This implies an equally high rate of longwave absorptivity because of Kirchhoff's law of thermal radiation (Kirchhoff, 1860), making snow susceptible to greater

heating due to downwelling longwave radiation from clouds (Zhang et al., 1996). Snow fields tend to have low thermal conductivities (from 0.1 to $0.5 \text{ W m}^{-1} \text{ K}^{-1}$) which increase with density due to the fact that a large portion of most snow layers is air (Zhang, 2005). This low conductivity contributes to a strong insulating effect between the atmosphere and the soil surface beneath the snow. The strongest cooling is typically confined to a shallow layer near the surface which increases boundary layer stability and inhibits vertical fluxes such as that of sensible and latent heat (Cohen and Rind, 1991).

Latent heat is the energy exchanged from the phase changes of water. Snowmelt is an exceptional sink of latent heat energy because the latent heat of fusion required to melt ice is two orders of magnitude greater than the heat capacity of ice (Zhang, 2005). Even when latent heat released by condensation to the snow's surface (Wallen, 1949) contributes to melting the snow, the ground surface remains at 0°C or below due to the latent heating effect (Zhang et al., 1997). While latent heat flux is generally directed from the surface to the atmosphere when snow is present, the magnitude is greater when albedo is lower due to a warmer surface which allows greater accessibility to melting and sublimating snow (Ellis and Leathers, 1999). These processes appear to contribute to a positive feedback which increases snowmelt during warm conditions and inhibits it during cold conditions.

Horizontal temperature gradients (and thus, density gradients) contribute to the available potential energy (APE) of a system which may be converted into momentum. In this context, APE is regarded as baroclinic instability (Grotjahn, 2015), defined as a misalignment of the pressure and density gradients of a stratified fluid and proportional to their cross product. The thermal wind balance suggests that these baroclinic zones, characterized by horizontal temperature gradients, are also characterized by vertical wind shear. Sobolowski et al.

(2010) found that by forcing extensive snow covers over North America in the ECHAM5 atmospheric general circulation model, the meridional temperature gradient over the continent was strengthened in the south, contributing to enhanced baroclinicity which would then propagate downstream. The strongest response to forced snow covers occurred in spring (Sobolowski et al., 2010) though the ECHAM5 surface albedo parameterization does not include consideration of seasonal variations in snow albedo caused by the snow's age (Roeckner et al., 2003). Rydzik and Desai (2014) found that low-level baroclinicity in the months from November to March reaches maximum values in a region up to 350 km south of the southern extent of snow.

1.1.3 Atmospheric Moisture

The flux of water vapor into the atmosphere from the surface is diminished when snow cover is present (Ellis and Leathers, 1999). Observations have shown that evaporation and sublimation from snow fields are minimal (Bergen and Swanson, 1964; Persson, 1975) and often outweighed by condensation of water vapor to the snow (West and Knoerr, 1959). Highly stable conditions tend to prevent much vertical transport of water vapor over snow cover (Bengtsson, 1980) though this may be overcome by turbulent eddies in the boundary layer (Sverdrup, 1936). When local snow cover is close to 100%, ecosystem evapotranspiration is nearly zero, except when snow melt is occurring (Black et al., 1996). Snow cover has been found to inhibit precipitation in observations (Namias, 1985) and modelling studies (Waland and Simmonds, 1996; Elguindi et al., 2005), likely due to variations in static stability of the lower atmosphere and the lack of upward moisture flux. Snowmelt, however, appears to contribute to enhanced precipitation (Namias, 1985).

1.2 Snow Cover Trends

Countless sources have noted a consistent trend of rising surface and near-surface air temperatures globally from the late 19th Century to the present (Jones, 1988; Folland et al., 2001; Rayner et al., 2003; Hansen et al., 2006). Recent rising temperatures anomalous in the broader 300 year context have been observed in North America in conjunction with rising concentrations of atmospheric CO₂ (Jacoby and D'Arrigo, 1989). Analyses of projected twenty-first century GCM outputs indicate that this trend of warming mean surface air temperatures in North America will continue (Maloney et al., 2014) with the largest increases in winter (Plummer, 2006). The upward trend in surface air temperatures has straightforward implications for the behavior of snow accumulation and melt which are closely associated with a 0°C threshold. Simplified general circulation model experiments have shown that substantial increases in atmospheric CO₂ concentration contribute to a poleward retreat of snow cover (Manabe and Wetherald, 1980).

1.2.1 Historical and Present

Snow cover on the North American landmass has been decreasing since the mid-twentieth century, particularly in spring (Brown, 2000; Lemke et al., 2007; Gan et al., 2013). This trend has persisted into the early twenty-first century with snow cover decreasing more in the southern latitudes of the Northern Hemisphere (Li et al., 2018), effectively shifting the southern extent of snow further north. The observed decrease in wintertime surface albedo has been attributed to a decrease in snow cover rather than variations in the state of the snow itself (Qu and Hall, 2007). A strong linear correlation has been noted between recent reductions in spring snow cover extent and surface air temperatures (Brutel-Vuilmet et al.,

2013). This negative correlation is strongest in the region of the Great Plains encompassing Nebraska, South Dakota, and southeast Montana, where snow cover variability is highest (Robinson and Hughes, 1991). In winter, North American snow extent is highly correlated with tropospheric dynamics from which it becomes decoupled in spring, making surface temperature the dominant factor (Frei and Robinson, 1999).

1.2.2 Projected

Brown and Mote (2009) found from analysis of CMIP3 model output that snow cover duration and maximum snow water equivalent (SWE) values throughout North America are projected to decrease as the twenty-first century progresses, though the signal is not as strong in the Great Plains as it is in coastal or mountainous regions. Peacock (2012) found through the use of the Community Climate System Model, version 4 (CCSM4) that seasonal snow cover would decrease throughout the twenty-first century, especially during spring. Brutel-Vuilmet et al. (2013) found through analysis of the CMIP5 suite that the relative retreat of spring snow cover extent was dependent on the radiative forcing caused by the concentration of greenhouse gases (GHGs), as shown in Figure 1. Simulations show twenty-first century increases in snowfall in mid- to high-latitude regions due to increased precipitation (Peacock, 2012; Maloney et al., 2014) where temperatures are unlikely to exceed 0°C in winter, despite negative mean trends in snowfall globally (Räisänen, 2007; Kapnick and Delworth, 2013, Krasting et al., 2013). There may also be local increases in lake-effect snowfall in the Great Lakes region as a result of reduced ice cover (Burnett et al., 2003) though more recent analysis suggests that the increased lake-effect precipitation will manifest as rainfall rather than snowfall with heavy lake-effect snowstorms declining in frequency but increasing in

intensity by the late twenty-first century (Notaro et al., 2015). Rhoades et al. (2018) note that for high-GHG concentration experiments of the variable-resolution Community Earth System Model (VR-CESM), snowfall, snow cover, and SWE do not decrease at elevations higher than 2,000 m in the late 21st century (2075-2100) when compared to the historical simulations (1980-2005).

1.3 Extratropical Cyclones

The American Meteorological Society (AMS) *Glossary of Meteorology* (2018) defines an extratropical cyclone as a synoptic scale cyclonic circulation which is not tropical. The term typically refers to migratory closed circulations (vortices) which occur in the middle or high latitudes and do not originate over tropical oceans. Included in this broad definition are subtropical and midlatitude cyclones. Extratropical cyclones are major contributors to much of the most impactful weather in North America, including high wind, extreme cold, and heavy precipitation events (Ma and Chang, 2017).

Extratropical cyclones contribute substantially to precipitation on the North American continent. In most of the Great Plains region, the contribution exceeds 80% of the total amount of winter (December through February) precipitation, even exceeding 85% in certain areas (Hawcroft et al. 2012). That value surpasses 50% in every other part of the continent. Over 20% of the precipitation associated with wintertime extratropical cyclones accompanies just 10% of storms. The percentage of storm associated precipitation decreases for summer months but still exceeds 50% in the Great Plains (Hawcroft et al. 2012). Generally, an estimated 70% of the moisture in extratropical cyclones comes from the surrounding atmosphere and the remaining 30% is obtained by surface evaporation (Trenberth, 1998).

Bjerknes and Solberg (1922) identified a sharp air temperature gradient of cold polar air against warm tropical air along which cyclonic vortices would appear. As a cyclone progresses through its life cycle, as outlined by this Norwegian Model, it deepens and deforms this polar front through the advance and eventual occlusion of its warm and cold fronts. This baroclinic instability or vertical wind shear in the lower troposphere can be shown to contribute to the generation of vorticity and the development of storm tracks (Inatsu et al., 2002) and winter cyclones statistically favor movement along areas of high baroclinicity which are found just south of the extent of snow (Rydzik and Desai, 2014).

1.3.1 Projected Trends

Analyses of GCM outputs indicate a poleward shift in many Northern Hemisphere winter cyclone storm tracks in the twenty-first century (Yin, 2005; Teng et al., 2008; Maloney et al., 2014). Storms are not projected to become more intense and the frequency of the storms is expected to diminish somewhat (Geng and Sugi, 2003; Bengtsson et al., 2006). While certain regions of the Northern Hemisphere, namely the Central Pacific, undergo dramatic poleward shifts in cyclone tracks, the modelled response in the Great Plains is minimal, though not negligible (Bengtsson et al., 2006). The apparent reason for the decrease in cyclone frequency and intensity, as well as the poleward shift, is a change in baroclinicity brought about by a relaxation of the poleward temperature gradient caused by the warming of the Arctic (Geng and Sugi, 2003; Bengtsson et al., 2006). These changes in North America, projected by GCM output, do not substantially differ in more recent studies using the CMIP5 model suite (Wuebbles et al., 2014).

Using a five-member ensemble of version 3 of the Community Climate System Model (CCSM3) for the twentieth and twenty-first century, Finnis et al. (2007) found an increase in daily precipitation associated with extratropical cyclones due to an increase in available atmospheric moisture caused by higher temperatures. This outcome was found to be strongest at high latitudes while the effect in the midlatitudes was lessened by a reduction in cyclone frequency.

1.4 Cyclones and Snow Cover

Because Sutcliffe (1947) had shown that upper air divergence, and thus upward vertical motion, is forced by the advection of cyclonic vorticity by the thermal wind, a framework had been provided for meteorologists to consider whether snow field boundaries which contribute to steep thermal gradients (baroclinic zones) could play a role in cyclone steering. Lamb (1955) found that broad areal extents of snow would limit the movement of 1,000-500 hPa isopleths and maintain an upper-tropospheric trough over that location. From this, Lamb reasoned that such snow fields could limit the movement of cyclones, writing that, "An established continental snow-cover in any winter may be expected to encourage the steering of depressions along its perimeter."

Namias (1962) provided analysis of observations to support a similar hypothesis showing that the abnormally extensive North American snow cover in the period from February to March of 1960 contributed to unexpectedly low temperature and thickness anomalies up to 700 hPa and a higher than average sea-level pressure over the continent contributing to a large anticyclone. The greatest forecast errors in temperature occurred closest to the boundary of snow cover, indicating the strong influence on temperature that snow cover has

even at the margins of its areal extent. Namias further noted that during this period, a large number of rapidly developing and occluding east coast cyclones (Nor'easters) travelled and intensified along similar paths. Namias concluded that this was due to the high baroclinicity caused by the temperature contrast between air overlying the abnormal extent of snow and the warm coastal waters of the Gulf Stream.

Dickson and Namias (1976) subsequently showed that periods of great continental warmth or cold in the American Southeast had a direct influence on the strength of the baroclinic zone on the coast and would affect the average frequency and positions of Nor'easters, drawing them further south when the Southeast was colder. Dickson and Namias also noted that storm frequency was greater in the northern Great Lakes region during warmer winter periods, hinting that smaller extents of snow may favor greater development of "Alberta Clipper" tracks, which form in the lee of the Canadian Rockies and proceed toward the Great Lakes (Thomas and Martin, 2007). Heim and Dewey (1984) showed that extensive snow cover contributed to a greater frequency of cyclones in the southern Great Plains and Southeast and a reduction in the amount of cyclones further north.

Ross and Walsh (1986) studied the effects that the snow extent margin had on 100 observed North American cyclone cases which moved parallel to the baroclinic zone within 500-600 km of the snow margin by measuring forecast error from a barotropic model, which does not account for baroclinicity in the generation of vorticity. Ross and Walsh were able to determine that the baroclinicity associated with the snow boundary was an important factor in cyclone steering and intensity, one which was more pronounced for coastal areas than further inland. These findings could only be applied to cases which were already within the prescribed distance from the snow extent boundary.

Walland and Simmonds (1997) ran GCM experiments with forced anomalously high and low realistic snow cover distributions. Walland and Simmonds noticed a reduction in North American cyclones when the snow cover was more extensive but cyclone densities were located further south, similar to the observations of Heim and Dewey (1984).

Elguindi et al. (2005) reduced the field of study to the Great Plains region by using a 25-km-resolution nested domain within the Penn State-NCAR Mesoscale Model (MM5) and simulating eight well-developed cyclone cases. Elguindi et al. found that after filling the entire inner domain with snow and employing a 48-hour spin-up period, all cyclone cases experienced an increase in central pressure and decrease in precipitation, while most experienced a decrease in the cold front temperature gradient. The greatest effect of cooling and drying was experienced in the warm sectors of the perturbed case simulations causing an increase in atmospheric stability and a subsequent decrease in precipitation and cloud cover. This experiment yielded some changes in cyclone trajectory though they were highly variable and inconsistent with regards to snow cover changes.

1.5 Motivation for this Study

Many authors have used global and regional climate models to study the projected behavior of extratropical cyclones in the late twenty-first century (e.g. Maloney et al., 2014) but few if any have examined the contribution made solely by the projected extents of snow cover. While many observational and modelling studies have analyzed the effects of extensive distributions of snow cover on cyclone behavior (e.g. Namias, 1962; Heim and Dewey, 1984; Elguindi et al., 2005), few have explicitly studied the effects of reductions in snow cover such as Walland and Simmonds (1984) who did not experiment with projected

snow cover extents. A few studies have suggested the importance of the snow extent boundary to cyclone behavior (e.g. Ross and Walsh, 1986; Rydzik and Desai, 2014) though there haven't been modelling studies which experiment with shifts explicitly applied to these boundaries. While the pronounced effects of snow cover in the Great Plains has long been well understood and while regional modelling with snow forcing has been applied to the area (Elguindi et al., 2005), regional climate studies in the Great Plains focusing on projected snow extent retreat have not been accomplished. Finally, the great deficiency in all such regional, case-oriented modelling studies performed to date is the dependence on a small number of simulations. Examining several simulations across greater numbers of cases not only provides the statistical robustness of a large dataset but also allows the ability to examine the differences in individual simulations not afforded to broader climatological studies.

The aim of this study is to isolate the direct, short-term effect of twenty-first century snow cover extents on twentieth century extratropical cyclones over the Great Plains in winter and spring by shifting the southern boundary of snow poleward according to values of snow retreat from the late twentieth to the late twenty-first century. Through large ensemble modelling of several subjectively-selected cyclone cases, this study seeks to answer the following questions:

- What effect will shifted snow boundaries have on individual cyclone trajectories and intensities?
- What effect will these changes have on precipitation associated with cyclone cases, particularly where large populations are concerned?

- To what extent are these effects dependent on the position of the snow boundary, the duration of the newly-established snow cover, the total amount of snow removed, and the time of year?

2 Data and Methods

2.1 Domain

The study focuses on the Great Plains region of North America. This area was chosen because of its high inter- and intra-annual variability of snow cover (Robinson, 1996), because the flat topography and relative lack of trees eliminates consideration of their influences on cyclone cases, because cyclones frequently travel across the region in winter due to enhanced cyclogenesis in the lee of the Rocky Mountains (Zishka and Smith, 1980), because the correlation between snow cover and negative temperature anomalies is stronger in the Great Plains than anywhere else in North America (Heim and Dewey, 1984), and because the region represents one of the largest disparities between maximum snow albedo and background surface albedo on the North American continent (Figure 2).

The model domain established was a 30 km resolution grid spanning 6,300 km west-to-east and 4,320 km south-to-north (210×144) on a Lambert conformal conic projection centered on 43.5°N 98°W with true latitudes at 30°N and 60°N (Figure 3). The model was configured to include 30 vertical eta levels (step-like, terrain-following) between the land surface and the 100 hPa pressure level. Lateral boundary conditions were specified at the margins with a four grid cell (120 km) relaxation zone with no nudging. The domain was chosen to include the climatological tracks of Alberta Clipper and Panhandle Hook cyclones

(Zishka and Smith, 1980; Thomas and Martin, 2007) with enough space provided to allow for anomalous trajectories which wouldn't be influenced by boundary conditions.

2.2 Case selection

20 extratropical cyclone cases were selected subjectively by examining 3-hourly North American Regional Reanalysis (NARR) weather maps published online by the Penn State Department of Meteorology (<http://mp1.met.psu.edu/~fxg1/NARR/>). 4 cases were chosen within the years from 1986-2005 for each month between November and March such that the time from four days prior to cyclogenesis to the hour of cyclolysis (or the cyclone leaving the domain) did not cross over into another month. Cyclone trajectories had to be far enough from the domain borders to ensure that boundary conditions would not dictate their behavior.

A diverse range of characteristics were sought for the cases. Of particular interest was the region of cyclogenesis and the trajectory which each cyclone took. Foremost, cyclones had to track over or near the Great Plains region. Cases were preferred if cyclogenesis took place in the lee of the Northern Rocky Mountains and near the western end of the Oklahoma panhandle, two of the regions of most frequent cyclogenesis (Reitan, 1974; Zishka and Smith, 1980). Cyclones with different intensities, determined by minimum sea-level pressure, and upper-level forcings, determined subjectively by examining 500 mb curvature and vorticity advection, were sought. The objective was to assess the effect of removed snow cover on as many different types of storms as possible. Of the 20 selected cases, the control simulation results of only 15 were deemed to be consistent enough with observations to warrant analysis in this study. Unfortunately, this left many Alberta Clippers and few Panhandle Hook cyclones. The paths of all 15 cases are plotted simultaneously in Figure 4.

2.3 Data

2.3.1 *North American Regional Reanalysis*

The North American Regional Reanalysis (NARR; Mesinger et al., 2006) is a high-resolution, high-frequency dataset from the National Centers for Environmental Prediction (NCEP) which contains data from 1979 to the present for the North American domain. The reanalysis is comprised of assimilated data from the Regional Data Assimilation System (RDAS) and output from the NCEP Eta Model at 32 km resolution on a northern lambert conformal conic grid. The domain size is 349 by 277 grid spaces with 45 vertical layers. The data are available in 3-hourly, daily, and monthly composites.

The NCEP Eta Model makes use of the Noah land surface model (*see section 2.4.1*; Ek et al., 2003) to simulate the snowpack states of snow water equivalent (SWE), density, and fractional coverage by calculating sublimation, snowfall, and snowmelt as well as the surface energy fluxes due to radiation, sensible and latent heat flux, subsurface heat flux, and phase-change heat sources and sinks (Mesinger et al., 2006). Snow data assimilation is done primarily with satellite data (K. Mitchell, NCEP/Environmental Modeling Center, 2008, personal communication, as cited in Salzmann and Mearns, 2012). SWE is updated at 0000 UTC daily from the U.S. Air Force Weather Agency's SNODEP model output which utilizes station and satellite data as well as some manual interpretation (Kopp and Kiess, 1996).

The NARR data used for this study were provided in grib format by NOAA/OAR/ESRL PSD, Boulder, Colorado, USA, at <https://www.esrl.noaa.gov/psd/>. 3-hour NARR data were used to initialize and set boundary conditions for the WRF model simulations as well as provide context for historical (1986-2005) monthly snow line averages.

2.3.2 CMIP5

The fifth phase of the Coupled Model Intercomparison Project (CMIP5; Taylor et al., 2012) is a collaboration of the 12th Session of the Working Group on Coupled Modelling (WGCM) of the World Climate Research Programme (WCRP) in support of the Intergovernmental Panel on Climate Change's Fifth Assessment Report (IPCC AR5). With over 30 coupled climate models, the goal of the project was to promote a standard set of long- and short-term model simulations to evaluate individual model accuracy in simulating the past, provide future projections under different conditions, and understand the reasons for disagreement among models (Taylor et al., 2009). Among experiments for future simulations are the Representative Concentration Pathways (RCP; van Vuuren et al., 2011), which are a set of four greenhouse gas concentration trajectories contributing to separate radiative forcing values (+2.6, +4.5, +6.0, and +8.5 W m⁻² relative to pre-industrial values) in the year 2100. Each represents evolving emissions scenarios for the twenty-first century and beyond with RCP2.6 representing a dramatic global shift away from fossil fuel use and RCP8.5 representing an increasing trend of fossil fuel use described as “business as usual.”

This study utilizes model output from historical, RCP4.5, and RCP8.5 experiments which, as members of the core set of experiments, were present for all models. RCP2.6 and RCP6.0 are not core experiments of the CMIP5 project and have not been simulated by all models. Selected models were chosen from Brutel-Vuilmet et al. (2013) who found that the CMIP5 models they had analyzed were able to faithfully reproduce observed snow mass (also SWE) extent from 1979-2005, except in spring where the models underestimated the significant long-term reduction over time. Brutel-Vuilmet et al. analyzed SWE data from 22

models, the only ones with land and ice sheet masks available. Certain models were removed from consideration in this study for a variety of reasons. The BCC-CSM1.1 model was omitted for not having monthly-averaged snow mass data readily available. The CanESM2 model was excluded from this study due to its exceptionally large lake mask in the Great Lakes region which tended to contribute to unrealistic snow line assessments at those longitudes. The RCP4.5 experiment data were not available for the FGOALS-g2 model. The MIROC-ESM and MIROC-ESM-CHEM models had spatial resolutions that were too coarse for the snow extent algorithm to interpolate to the domain used for the regional model. In the end, 14 models were considered for determining projected snow extent distributions (Table 1). Many models had multiple realizations and a few different physics options simulated which were averaged together for individual models and then all different models, even if associated with the same institutions as other models, were treated separately.

2.4 Model Physics

Cases were simulated with NCAR's WRF version 3.9 (Skamarock et al., 2008), which is a numerical weather prediction (NWP) model with interchangeable physics options. Simulations employed the Advanced Research WRF (WRF-ARW) dynamical solver which involves fully compressible, time-split 2nd- to 3rd-order Runge-Kutta integration on an Arakawa C grid on a stretched, terrain-following vertical coordinate (a full summary of the model protocols and governing equations can be found in Skamarock et al., 2008).

This study employed standard physics options with efficiency and accuracy in mind with some alterations made to the land surface model (*see section 2.4.1*). The WRF Single-Moment 3-class (WSM3) scheme (Hong et al., 2004) was used to parameterize microphysics

which allows for water vapor, cloud water/ice, and rain/snow hydrometeors and the various transitions between them.

2.4.1 Noah Land Surface Model

Of the land surface schema available for use in WRF, the NOAH land surface model (Noah; LSM; Mitchell et al. 2001) was chosen. The Noah LSM is widely used in weather and climate models by such organizations as NCEP and the National Weather Service (NWS). Noah itself is an acronym of the organizations NCEP, Oregon State University, the Air Force Weather Agency and Air Force Research Lab, and the NWS Hydrology Lab. The model's performance has been extensively researched and its strengths and limitations are well understood.

The Noah LSM uses a single layer snow model and calculates snow albedo by means of the method employed by Livneh et al. (2010), which calculates the albedo of the snow-covered portion of a grid cell as

$$\alpha_{snow} = \alpha_{max} A^t B$$

where α_{max} is the maximum albedo for fresh snow in the given grid cell (established by data from Robinson and Kukla, 1985), t is the age of the snow in days, and A and B are coefficients which are, respectively, 0.94 and 0.58 (0.82 and 0.46) during periods of accumulation (ablation). The decay of the fraction of α_{max} by day during accumulation and ablation phases is shown in Figure 5. In current versions of the WRF Noah LSM, two issues prevent the ideal execution of this formula: first, the coefficients A and B are fixed and may only be changed by recompiling the model, leaving them set to either the accumulation or ablation phase of snow and second, t is always set to zero at model initialization. In this way,

to determine the albedo of the snow in a grid cell, the WRF Noah LSM module treats all snow as newly-fallen snow which is either accumulating or ablating. This can lead to an overestimation of surface albedo in high-resolution simulations of ablating snow fields, causing a significant underestimation of 2-m temperature accompanied by an overestimation of outgoing shortwave radiation (Tomasi et al., 2017).

In order to address the issue of the accumulation/ablation coefficients, two versions of WRF were compiled. The first had values for A and B set to those for accumulating snow and was used for cases taking place in November through February. The second version of WRF had A and B set to their corresponding values for ablation and was only used for cases taking place in March. The issue of the snow's age was not addressed, which may result in a stronger albedo and temperature gradient than would otherwise be present.

The albedo, α , of the entire grid cell is determined from the snow albedo by the equation

$$\alpha = \alpha_0 + f_{snow}(\alpha_{snow} - \alpha_0)$$

where α_0 is the background snow-free albedo of the grid cell which is determined by the day of year and does not account for vegetation and f_{snow} is the fraction of the grid cell covered by snow (fractional snow cover; FSNO). If the value for the background snow-free albedo is higher than the calculated value for snow albedo, the total grid cell's albedo is set to that for the background snow-free albedo. The emissivity, ε , of the grid cell is calculated similarly as

$$\varepsilon = \varepsilon_0 + f_{snow}(\varepsilon_{snow} - \varepsilon_0).$$

FSNO is quite often a limiting factor in a grid cell's albedo and emissivity and is calculated thusly:

$$f_{snow} = 1 - (e^{-\lambda R} - R \cdot e^{-\lambda})$$

such that R is the ratio of SWE to the threshold value for a grid cell's SWE above which snow cover is total and λ is a tuning parameter equal to 4 (since the release of Noah LSM version 2.6; Mitchell et al., 2005).

The thermal conductivity of snow for a grid cell is calculated in $\text{W m}^{-1} \text{C}^{-1}$ from a basic version of the Dyachkova and Serova equation (1960; as referenced in Golubev and Frolov, 2015) which is valid for snow densities between 0.1 and 0.4 kg cm^{-3} :

$$k_{snow} = 0.0763 \cdot 10^{2.25\rho_s}$$

Here ρ_s is the density of the snow which can be calculated simply as SWE divided by the snow depth. Thermal conductivity determines the magnitude of soil-snow heat flux, calculated as

$$G = k_{snow} \frac{T_{skin} - T_{soil}}{D_{snow}}$$

where D_{snow} is the snow depth and T is the temperature of the land surface and the top soil level, respectively.

Precipitation is categorized as snow if the fraction of frozen precipitation passed in from the microphysics scheme is greater than 50%. If precipitation is liquid but the skin temperature is freezing or below, the precipitation is categorized as freezing rain. No snowmelt occurs in the surface temperature is at or below freezing. Sublimation and frostfall are governed entirely by the sign of potential evaporation [$\text{kg m}^{-2} \text{s}^{-1}$] which is fed in from the model.

2.5 Experimental Design

For each of the 15 cases, 25 simulations were run for a total of 375 distinct simulations. Each case was simulated at 5 initialization times: 0, 24, 48, 72, and 96 hours prior to cyclogenesis in order to determine for how long a snow cover must be established to elicit a change in cyclone behavior. The time of cyclogenesis for each case was subjectively determined by analysis of sea-level pressure (SLP) charts in NARR data. At each initialization time, 5 separate snow distributions were tested: the control case with observed snow cover, the tenth, fiftieth, and ninetieth percentiles of projected northward snow retreat (*see section 2.5.2*), and a sensitivity test where all snow in the domain is removed. Removing all snow in the domain is intended to reveal the extent to which cyclones are affected by shifting snow boundaries as opposed to the simple removal of snow.

2.5.1 *Snow line determination*

The snow line is defined here as the continuous lateral boundary demarcating the southernmost extent of snow-covered ground across the North American continent at a given instant or averaged over a given time period. The month-averaged snow line was objectively determined for each realization of each of the 14 CMIP5 models for each month between November and March for the years between 2080 and 2099. Values within the same month across all years and realizations for each model were then averaged to produce ten average snow lines per model, one for each RCP experiment for each of the five months. One snow line for each model was similarly determined for each month of the historical experiment between the years of 1986 and 2005.

The algorithm to determine the snow line of a retrieved snow extent begins at the western end of the domain and moves eastward at each step as it scans from south to north. A grid cell is considered to be snow-covered if the SWE is equal to or exceeds 5 kg m^{-2} (as in Brutel-Vuilmet et al., 2013). When the algorithm identifies a grid point with SWE exceeding 5 kg m^{-2} , it looks at all grid points between there and 300 km to the north (equivalent 2.7° latitude). Capping all SWE values at a maximum value of 6 kg m^{-2} , the algorithm takes the average of all points within the span and, if the value exceeds 5 kg m^{-2} , the snow line value for that longitude is set to the first (southernmost) point in the span and the algorithm scans at the next longitude. This method prevents the algorithm from identifying rogue southern patches of snow as being part of the greater continental snow extent while also allowing some minor irregularities at the snow margin. Once the exact snow line is determined, a 20-point (600 km) moving average is applied to smooth the result.

SWE was chosen for the snow line algorithm over FSNO and snow depth for a host of reasons. Brutel-Vuilmet et al. (2013) have determined that the mean ensemble of CMIP5 members reproduced historical SWE very well except in spring, where the reduction in SWE over time was underestimated. This reproduction of snow coverage was determined according to a 5 kg m^{-2} threshold of SWE which is why the same threshold it utilized for this study. There is no standard formula for the determination of FSNO, even among members of the CMIP5 experiment, rendering comparisons between models less meaningful. FSNO is also based largely on surface roughness, making it subject to mountain ranges, forests, and urban areas, creating a patchy distribution which does not easily lend itself to determining a southern extent. The WRF Noah LSM determines FSNO from inputs of SWE rather than snow depth, making SWE more relevant to albedo as well as energy and moisture fluxes.

2.5.2 *Snow Removal*

Once each CMIP5 model had a historical (1986-2005), and projected RCP4.5 and RCP8.5 (2080-2099) average snow line determined for each month, the meridional distance was determined between historical and projected snow lines at each zonal location, producing δ -arrays. The δ -arrays store the distance between two corresponding points on a historical and projected snow line. The δ -array method was used as opposed to inserting actual projected future snow cover distributions in order to gauge the response of cyclones to quantified shifts in snow lines and bypass the effect of model bias. It is necessary when working with future climate projections to assume that bias present in historical simulations will persist in future simulations in order to make meaningful interpretations of prospective changes (Peacock, 2012). A δ -array does not tell us what a future snow line will look like but rather how much a model predicts the average snow extent will recede.

With two δ -arrays for each model, RCP4.5 and RCP8.5, snow retreat values were averaged across a 3,000 km distance which spanned roughly from the central Rocky Mountains to the eastern seaboard according to zonal values on the conformal grid, ignoring snow retreat values in the Great Basin and Pacific Coast as well as those in New England and the Canadian Maritimes. Among these average values for each month, the tenth, fiftieth, and ninetieth percentiles of reduced snow extent were determined (Figure 6, Table 2).

In order to test the effect of the tenth, fiftieth, and ninetieth percentiles of snow extent retreat, a simulation with these adjustments was run for each case. In order to make the necessary adjustment, values from δ -arrays corresponding to the month of the case being tested were applied to that case's observed snow extent. By adding retreat values to each

zonal location on the observed snow line, a new snow line is produced. Once the new snow line has been determined, the SWE and snow depth values to the south of it are set to zero, except where snow is above 2,000 m above sea level. In simulations where all snow is removed, these snow variable values are set to zero throughout the domain, including above 2,000 m in elevation. The area where snow is forcibly removed for each perturbed simulation is called the depopulated zone (DPZ).

One consequence of the snow removal method which should not be overlooked is the creation of an unnatural “hard margin” at the southern extent of the adjusted snow field. Most snow fields have gradual decreases in SWE and snow depth which may contribute to relaxed albedo, temperature, and moisture flux gradients contributed by the snow field at the boundary. The removal of all snow south of the perturbed snow line creates, in most areas, a sharp drop in SWE and snow depth which is likely to contribute to stronger gradients at the new snow line. This is not considered detrimental to the study as it is expected to create an exaggerated signal which must be qualified as such.

2.5.3 *WRF simulations*

Simulations for each case were run simultaneously using WRF in serial mode on multiple separate servers courtesy of the University of Wisconsin Center for High Throughput Computing. An initial “primer” simulation was run for each case, initialized 96 hours prior to cyclogenesis and run through cyclolysis, which produced restart files for every 24-hour interval. These restart files were used to initialize both control and perturbed model simulations in the high throughput environment. The primer runs differed from the control runs initialized four days out because unlike control runs, primer runs were initialized with

true snow cover observations on the day of initialization. Regardless of initialization time, all non-primer simulations were initialized with the snow cover present at the time of cyclogenesis before any alterations were applied. This was so that all initialization times would use identical snow cover distributions in order to remove the effects of day-to-day snow cover variability.

In order to isolate the influence of established snow cover as opposed to snow deposited ahead of a cyclone by itself and to retain consistent snow distributions for altered cases, especially where no snow cover is present, the Noah LSM was edited so that snow does not accumulate on the ground. To be clear, this does not prevent snowfall from reaching the ground nor does it alter the phase of frozen precipitation as in Vavrus (2007); rather, it permanently sets the variable in the LSM for snow accumulation at the surface to zero.

2.5.4 Cyclone tracking

Because there were a limited amount of subjectively-selected cases used in this study, finding and tracking cyclone centers could be done without many of the challenges which broader and more long-term studies have faced (e.g., Geng and Sugi, 2003; Rydzik and Desai, 2014). Because the hour and general location of cyclogenesis were known for each case by examination of the NARR observation data, the simple cyclone-tracking algorithm was able to search within a square centered on a “guess point” in the domain grid for the minimum SLP in the area. Each side of the search box was 600 km in length, creating a $36 \times 10^4 \text{ km}^2$ area to search for a cyclogenesis location which may have shifted due to model error. Once the algorithm had found the first location of the cyclone trajectory, it would create a new search rectangle 975 km zonally by 900 km meridionally which was shifted so

that the previous cyclone center was 225 km from the western edge. The algorithm would then search the rectangle for the minimum SLP and renew the process until a specified time of cyclogenesis or until the cyclone center got too close to the domain boundary.

3 Results

3.1 Snow cover trends

δ -array averages indicate the mean retreat of snow from the period of 1986-2005 to 2080-2099 projected by each model within the span defined in subsection 2.5.2. Figure 6 shows the spread of all models for both RCP experiments for each month. The results show great disagreement among models with large, overlapping spreads though some trends are clear. All models for both experiments in all months show a projected poleward shift in snow cover extent, with a minimum average retreat in January of 50.7 km and a maximum in November of 1,025.4 km. The CMIP5 models show that the shoulder months of November, December and March experience greater retreats than those in the middle of winter.

Generally, RCP8.5 simulations show greater retreat than RCP4.5 though all months have multiple exceptions. According to the student's t-test, RCP8.5 experiments experience greater retreat within the 99.9% confidence interval except in March, where the confidence level shrinks to 99%. February has the lowest standard deviation of results at 175.6 km and December has the highest at 219.2 km. The standard deviation in November is comparable to that of December at 210 km. January and March are both comparable to February at 185.5 km and 183.9 km, respectively.

Perturbed snow fields are shown relative to the observed snow fields for each case in Figures 7, 8, and 9. The order of cases from left to right and top to bottom reflects the day of year on which the case takes place. The case on 1500Z 8 November 2005 has a snow extent which is so sparse and patchy that it is generally excluded from analyses involving direct comparison to the position of the snow line. The greatest extent of snow exceeding 5 kg m^{-2} occurs in the 2100Z 25 January 1996 case which is the only proper “Panhandle Hook” case and the southernmost path simulated in this study.

3.2 Pressure changes

Across all cases, initialization times, and snow cover alterations, 77% of simulations experienced an average decrease in pressure compared to the corresponding control simulation, however slight, and all perturbed simulations experienced some average change in pressure. Figure 10 shows the distribution of pressure changes averaged over the cyclone’s lifetime for perturbed simulations (perturbed-control). The mean average pressure change for all simulations was only -0.24 hPa. For cases initialized three and four days before cyclogenesis, the percent which experienced an average drop in pressure was 87%. The percentages are similar if only Alberta Clippers are examined. The maximum decrease in pressure during the cyclone’s lifetime is shown for all simulations in Figure 11. The average maximum pressure decrease is only 0.69 hPa but the maximum, which is quite anomalous, exceeds 7 hPa.

Average and maximum pressure changes do not correlate strongly with the amount of snow removed across all simulations ($R^2 = 0.22$ and $R^2 = 0.19$, respectively; $N = 300$ and $p < 0.01$ for both) nor if simulations with all snow removed are filtered out, even for simulations

with initialization three and four days out. Table 3 does show, however, that the percentage of simulations which have a negative average change in pressure is dependent on both the initialization time and the amount of snow cover removed with all 15 cases experiencing a decrease in average pressure when initialized at four days out with no snow. The simulations with the least amount of cases which experience an average pressure decrease are those which are initialized at cyclogenesis (T-0). Furthermore, when cyclones enter the DPZ, their central pressure decreases, on average, 247% as much as when not over the DPZ ($p < 0.001$). Depressions over the DPZ deepen an average of 396% as much as those which remain over snow ($p < 0.001$).

The response of central minimum SLP to snow removal is seasonally dependent, with stronger responses as the cold season progresses. Figure 12 shows the contrast in maximum pressure difference between control and perturbed simulations filtered by the periods of November-December (N=100), January-February (N=120), and March (N=80). The response is consistently weakest in the November-December period ($p < 0.001$) with an average maximum pressure decrease of -0.3 hPa. The response in the January-February period is much greater than that ($p < 0.001$) with an average of -0.7 hPa but the response is significantly greater in March than in the rest of the cold season ($p < 0.001$) at an average of -1.2 hPa. The four greatest pressure decreases all occur in March simulations, though they are outliers.

3.3 Trajectory departures

Every simulation experienced at least some mean trajectory deviation (MTD), determined as the sum of the total distances between corresponding points on control and perturbed paths

divided by the amount of three hour intervals in the cyclone lifetime. Figure 13 shows the distribution of MTDs across all simulations. The minimum amount experienced is 1.3 km (3h)^{-1} which occurred on a tenth percentile adjustment initialized three days prior to cyclogenesis and the maximum is $102.3 \text{ km (3h)}^{-1}$ which occurred as the result of a simulation with all snow removed and initialized four days prior to cyclogenesis. The average MTD across all simulations is $29.3 \text{ km (3h)}^{-1}$ with a standard deviation of $19.1 \text{ km (3h)}^{-1}$.

The cases which underwent large MTDs often accompanied large negative changes to average pressure ($R^2 = 0.45$, $p < 0.001$) and substantial maximum pressure decreases ($R^2 = 0.42$, $p < 0.001$). For cases initialized three or four days prior to cyclogenesis, the relationship to average pressure change becomes slightly more robust ($R^2 = 0.50$, $p < 0.001$). If only Alberta Clipper cases are considered, the relationship between MTD magnitude and maximum pressure decrease strengthens somewhat ($R^2 = 0.46$, $p < 0.001$).

Across-case averages for MTD for each adjustment amount and initialization time are given in Table 4. The case averages show that, while initialization time certainly has some influence in determining the magnitude of MTD, the outcome seems to be more dependent on the amount of snow removed. While the maximum value of across-case average MTDs for tenth percentile snow retreat simulations is $18.1 \text{ km (3h)}^{-1}$, the maximum average value for simulations initialized at the time of cyclogenesis (T-0) is more than double that and it is even exceeded by the average MTDs for the median snow retreat simulations at T-0. Figure 14 shows that MTD adheres fairly well to a linear relationship with the amount of snow removed across all cases ($R^2 = 0.47$, $p < 0.001$). If the simulations with all snow eliminated are filtered out, the relationship becomes much weaker ($R^2 = 0.27$, $p < 0.001$).

Like pressure, the trajectory deviation response is seasonally dependent, with stronger responses occurring later in the cold season. Figure 15 shows the mean trajectory deviation in km (3h)^{-1} across all simulations for the periods of November-December ($N=100$), January-February ($N=120$), and March ($N=80$). MTDs are significantly weaker in the November-December period ($p < 0.001$) with an average value of 21 km (3h)^{-1} . In the middle of winter, the average increases to $30.4 \text{ km (3h)}^{-1}$ and the values in March are significantly greater ($p < 0.001$), averaging 38 km (3h)^{-1} . Unlike the maximum pressure difference, the maximum outlier for the January-February period actually exceeds that of March and the two periods resemble one another more closely.

In order to determine whether cyclone trajectories were being steered toward or away from perturbed snow lines, the snowline-oriented trajectory deviation (SLOTD) was examined. SLOTD, like MTD, takes the average deviation between a perturbed and control path but, rather than sum up all deviations regardless of direction, the SLOTD algorithm finds the point on the snow line nearest each point on the perturbed trajectory and treats the deviation as positive if that point is closer to the snow line than the corresponding point on the control simulation's trajectory and negative otherwise. The average value for SLOTD across all simulations is 0.9 km (3h)^{-1} with a standard deviation of 4.3 km (3h)^{-1} . Values are similar for Alberta Clipper cases and cases initialized at least two days prior to cyclogenesis.

3.4 Precipitation changes

Storm-associated precipitation is calculated in a method similar to that presented by Hawcroft et al. (2012) who found that roughly 95% of precipitation associated with extratropical cyclones occurred within a 12° radial cap about the storm's minimum pressure

for the months of December, January and February. That same metric was used for the months of November and March in this study. Precipitation between unaltered and perturbed simulations were compared by subtracting the control storm's associated precipitation from that of the perturbed storm.

Almost exclusively, simulations initialized four days out experienced an increase in net storm-associated precipitation. The one exception was a simulation with all snow cover removed which also underwent substantial negative average and maximum pressure changes. Increases in total storm-associated precipitation grow in magnitude from tenth to ninetieth percentile snow perturbation experiments but for experiments with no snow, values were either higher than that of the ninetieth percentile removals or much lower. In many cases, the percentage of frozen precipitation decreased (often by an average of roughly 0.1%), while total precipitation increased, giving way to the generation of rain.

3.5 Snow line adherence

Case observations were tested for a property called adherence (A), which is a measure of the similarity of a cyclone's trajectory to and distance from the snow line. Adherence is essentially the average distance of the cyclone center from the snow line subtracted from the linear correlation of the cyclone trajectory to the snow line and is calculated as

$$A = \frac{[n \sum TS - (\sum T)(\sum S)]}{\sqrt{[n \sum T^2 - (\sum T)^2][n \sum S^2 - (\sum S)^2]}} - \left(\frac{e^{0.001d} - 1}{e} \right)$$

where T is the cyclone trajectory, S represents the corresponding points on the snow line, and d is the average distance, in kilometers, of the cyclone trajectory from its corresponding snow

line points. Adherence is high if the trajectory closely follows the snow line and low if the trajectory does not look like the snow line or if it is too far from the snow line.

When comparing the adherence of observed cyclone trajectories to the snow line from NARR observations and their minimum central pressure for each case, a robust linear relationship emerges such that the correlation coefficient is equal to -0.664 ($p < 0.01$; Figure 16). The value is similar if only Clippers are examined and far less ($r = 0.4$; $p > 0.05$) when examining average pressure of the cyclone. The relationship with average and maximum vorticity of the cyclone center is particularly weak and inconsistent (ranges from -0.021 to 0.209).

3.6 Changes for cities

Nineteen cities are examined in this study for temperature and precipitation changes to determine the effect of shifted snow line cyclone responses on large populations (Figure 17). Cities were chosen to be spread out and create a network of data points which are in or near the major cyclone tracks. All cities get warmer when snow is removed. The greatest warming is of minimum temperatures then mean temperatures. Maximum temperatures undergo some warming though often a fair amount less than the others. Minneapolis, in particular, warms far more than other cities in January and February (Table 5). At the same time, Minneapolis lies in or near the DPZ for all January and February cases.

The average change in storm-associated precipitation across all cases for fiftieth percentile simulations initialized four days prior to cyclogenesis were examined for all cities. For changes to rain and snowfall, as well as total precipitation, trends were inconsistent

across all cities and none of the changes were statistically significant ($p > 0.05$). Significance did not improve for ninetieth percentile perturbation simulations.

While precipitation statistics may not be generalizable for cities, certain cases do bare noteworthy results in perturbed simulations. For example, the “Panhandle Hook” case of 25 January, 1996 was a major precipitation event responsible for delivering a total of 19,041 cm of storm-associated precipitation along its trajectory, 48% of which was frozen. The northward shift of its exceptionally far southern snow line contributed to a considerable phase change in precipitation, particularly in the region around St. Louis, Missouri. The data show that for the ninetieth percentile shift, initialized four days prior to cyclogenesis, 2.1 cm of snow becomes 2.1 cm of rain in the city of St. Louis. For the tenth percentile shift, 1.3 cm of snow becomes rain. The numbers are similar when initialized three days out but drop off sharply when initialized two days or fewer out. Given enough time, even small shifts to the continental snow line contribute to a great enough temperature change to warrant a phase change in local precipitation.

4 Discussion

The retreat of snow extent calculated by comparing averages of historical (1986-2005) and late twenty-first century (2080-2099) snow lines is substantial, even in the tenth percentile of cases and there is unanimous agreement among all models that for both RCP experiments, the fall, winter, and spring extents of snow will recede by a minimum of an average 50 km. The snow extent retreats modelled in the RCP8.5 experiment are significantly ($p < 0.01$) greater than for the RCP4.5 experiment. There is considerable spread

in the retreats calculated in each month, indicating the inconsistency between models in precisely capturing the retreat of snow cover and meaning that the tenth, fiftieth, and ninetieth percentile perturbations in this study, while very different, are equally worthy of consideration. It may also not be entirely prudent to generalize by suggesting that tenth percentile cases represent RCP4.5 projected snow distributions since the tenth percentile snow retreat in both February and March are represented by model output from the RCP8.5 experiment. While Figure 6 indicates that greater average snow line retreat occurs in November and December than in March, it is important to recall that Brutel-Vuilmet et al. (2013) found that the CMIP5 suite consistently underestimates the reduction in spring snow cover extent. What's more, while there may be less retreat shown in March, snow in spring is both older and in its ablation phase, contributing to lower albedo and greater moisture availability than is present over new snow in the fall and early winter.

The pressure changes between perturbed and control cases shown have been minor. By adding snow to a mid-sized nested domain in the Great Plains only 48 hours prior to the transit of cyclones over the region, Elguindi et al. (2005) found an average minimum central pressure difference of 4.0 hPa, a threshold which only three simulations in this whole study exceeded. Perhaps this can be attributed to the fact that Elguindi et al. added snow as opposed to removing it or to the physics of the MM5 model compared to WRF-ARW. Even with the disparity in the magnitude of pressure changes, the trend of increasing central pressure when snow is added is complemented by the findings of this study where snow removal generally contributed to a decrease in central pressure. That cyclones experience significantly greater decreases in pressure while in transit over the depopulated zone

corroborates Elguindi et al. (2005)'s conclusion that snow cover prevents the deepening of midlatitude depressions.

The fact that observed adherence and minimum central pressure demonstrate a close linear relationship implies that pressure may be directly affected by the presence of snow margin baroclinicity. The negative correlation indicates that weaker storms are not more likely to follow the snow line but instead that the snow line may contribute to the intensification of storms which are near it. Further work should be done to investigate whether intensification of observed storms is closely tied to snow line adherence. It is unexpected that the vorticity field points toward no such relationship since the role of baroclinicity would be to contribute directly to the generation of vorticity.

The seasonal differences in the response of both pressure and MTD to snow removal are significant and cannot be ignored. The responses of both variables in the November-December period are incredibly small and the reason for which should be investigated further. The fact that the greatest responses are seen in March, the one month where the Noah LSM values for the Livneh et al. (2010) equation for snow albedo are set to the lower values for ablation, indicates that albedo is likely not the primary driver of this response even though solar zenith angle is higher in spring.

The relationship shown between MTD and pressure changes indicates that, while the two may not be directly linked, they do respond similarly to perturbed simulations. The neutral relationship of the snowline-oriented trajectory deviation to snow removal and low, inconsistent values indicates the snow line does not actively steer cyclones toward it for the most part; at least, not snow lines that have been established for four days or less. Tracking

cyclones by searching for SLP minima alone may provide an incomplete view of changes in the position of cyclones over time.

It is shown that snow cover has a cooling effect on cities, having particular influence on minimum temperatures as well as mean temperatures. This is especially noticeable when snow is removed from in and around the city in a perturbed simulation. This may indicate a feedback whereby a warmer future climate would reduce snow coverage for cities and contribute to greater warming in their respective locales.

The direct responses to short-term snow cover changes seen in the results of this experiment will not necessarily be present in the late twenty-first century as long-term adjustment to the reduced snow and feedbacks contributed by additional components of the climate system take effect. What's more, the "hard margin" of SWE created by the circumstances of snow cover removal in this study's methodology is expected to create a stronger baroclinic and moisture flux gradient than would realistically be present, especially coupled with the WRF Noah LSM's procedure to treat all snow as fresh at model initialization. These would be expected to increase the signal of removed snow on atmospheric circulation though the signals revealed by this study have been fairly weak. It may be that fixing these issues would provide a stronger response but it seems more likely that the real response by nature to sudden snow cover removal would be even less dramatic.

Finally, the decision to remove snow accumulation from precipitation at the surface may have been necessary in order to parse the influence of preexisting snow cover but may also exclude a potentially important feedback contributed by snow deposited from the storms themselves. However, due to the muted response in simulations initialized at the time of

cyclogenesis, it seems unlikely that snow deposited directly in front of or under an extratropical cyclone will have a strong effect on its behavior.

5 Conclusion

The WRF-ARW model was run for 15 separate extratropical cyclone cases with adjustments to the areal extent of snow, initialized zero to four days prior to cyclogenesis in order to determine the nature of the influence which the snow boundary exerts on these synoptic systems. Late twenty-first century snow extents were determined from future global projections with RCP4.5 and RCP8.5 greenhouse gas concentrations run by 14 models of the CMIP5 suite and all models across both experiments show that late twenty-first century snow coverage will be less than it was in the period from 1986-2005. The largest retreat of snow took place in November and then December but the GCMs have a tendency to underestimate snow extent retreats in spring. 77% of cases across all 375 simulations experienced an average decrease in pressure, though the magnitude was not high for most. Pressure was shown to decrease to a significantly greater degree while cyclones progressed through the area where snow had been removed and to remain closer to control values while over snow. Every simulation experienced some mean trajectory deviation, which was related somewhat reliably ($R^2 = 0.47$) to the amount of snow removed from the domain.

This work may be of use in short-term and subseasonal forecasting in determining how a cyclone may intensify with regards to a preexisting or recently-shifted snow field or what phase of precipitation one can expect, given the position of the snow line. Certainly,

forecasters should recognize the enhanced role which snow cover plays in cyclone steering and intensity in the month of March.

Weak responses to the removal of snow cover at the time of cyclogenesis suggest that the presence or absence of the snow margin has a minor though not entirely imperceptible immediate effect. There is little to imply that the effect on trajectory deviation, pressure change, or precipitation plateaus at T-4 simulations and so the question of the full scale of the snow margin's influence cannot be answered until longer case study simulations are executed.

6 References

- American Meteorological Society, cited 2018: Extratropical cyclone. Glossary of Meteorology. [Available online at http://glossary.ametsoc.org/wiki/Extratropical_cyclone].
- Baker, D. G., D. L. Ruschy, R. H. Skaggs, and D. B. Wall, 1992: Air temperature and radiation depressions associated with a snow cover. *Journal of Applied Meteorology and Climatology*, **31**, 247-254, doi:10.1175/1520-0450(1992)031<0247:ATARDA>2.0.CO;2.
- Bauer, K. G. and J. A. Dutton, 1962: Albedo variations measured from an airplane over several types of surface. *Journal of Geophysical Research*, **67**(6), 2367-2376, doi:10.1029/JZ067i006p02367.
- Bengtsson, L., 1980: Evaporation from a snow cover: review and discussion of measurements. *Nordic Hydrology*, **11**(5), 221-234, doi:10.2166/nh.1980.0010.
- Bengtsson, L., K. I. Hodges, and E. Roeckner, 2006: Storm Tracks and Climate Change. *Journal of Climate*, **19**(15), 3518–3543, doi:10.1175/JCLI3815.1.
- Bergen, J. D. and R. H. Swanson, 1964: Evaporation from a winter snow cover in the Rocky Mountains forest zone. *Western Snow Conference Proceedings*, 52-58.
- Black, T. A., G. D. Hartog, H. H. Neumann, P. D. Blanken, P. C. Yang, C. Russell, Z. Nestic, X. Lee, S. G. Chen, R. Staebler, and M. D. Novak, 1996: Annual cycles of water vapour and carbon dioxide fluxes in and above a boreal aspen forest. *Global Change Biology*, **2**(3), 219-229, doi:10.1111/j.1365-2486.1996.tb00074.x.
- Bjerknes, J. and H. Solberg, 1922: Life cycle and the Polar Front Theory of atmospheric circulation. *Geofysiske Publikationer*, **3**(1), 3-18.
- Brown, R. D., 2000: Northern Hemisphere snow cover variability and change, 1915-97, *Journal of Climate*, **13**, 2339-2354, doi:10.1175/1520-0442(200)013<2339:NHSCVA>2.0.CO;2.
- Brown, R. D. and P. W. Mote, 2009: The response of Northern Hemisphere snow cover to a changing climate. *Journal of Climate*, **22**, 2124-2145, doi:10.1175/2008JCLI2665.1
- Brutel-Vuilmet, C., M. Menegoz, and G. Krinner, 2013: An analysis of present and future seasonal Northern Hemisphere land snow cover simulated by CMIP5 coupled climate models. *The Cryosphere*, **7**, 67-80, doi:10.5194/tc-7-67-2013.
- Budyko, M. I., 1969: The effect of solar radiation of variations on the climate of the Earth. *Tellus*, **21**(5), 611-619, doi:10.3402/tellusa.v21i5.10109.

Carroll, J. J. and B. W. Fitch, 1981: Effects of solar elevation and cloudiness on snow albedo at the South Pole. *Journal of Geophysical Research: Oceans*, **86**(C6), 5271-5276, doi:10.1029/JC086iC06p05271.

Cohen, J. and D. Rind, 1991: The effect of snow cover on the climate. *Journal of Climate*, **4**, 689-706, doi:10.1175/1520-0442(1991)004<0689:TEOSCO>2.0.CO;2.

Dewey, K. F., 1977: Daily maximum and minimum temperature forecasts and the influence of snow cover. *Monthly Weather Review*, **105**, 1594-1597, doi:10.1175/1520-0493(1977)105<1594:DMAMTF>2.0.CO;2.

Dickson, R. R., and J. Namias, 1976: North American influences on the circulation and climate of the North Atlantic sector. *Monthly Weather Review*, **104**, 1255-1265, doi:10.1175/1520-0493(1976)104<1255:NAIOTC>2.0.CO;2.

Eaton, F. D. and I. Dirmhirn, 1979: Reflected irradiance indicatrices of natural surfaces and their effect on albedo. *Applied Optics*, **18**(7), 994-1008, doi:10.1364/AO.18.000994.

Ek, M. B., K. E. Mitchell, Y. Lin, E. Rogers, P. Grunmann, V. Koren, G. Gayno, and J. D. Tarpley, 2003: Implementation of Noah land surface model advances in the National Centers for Environmental Prediction operational mesoscale Eta model. *Journal of Geophysical Research*, **108**(D22), doi:10.1029/2002JD003296.

Elguindi, B. Hanson, and D. Leathers, 2005: The effects of snow cover on midlatitude cyclones in the Great Plains. *Journal of Hydrometeorology*, **6**, 263-279, doi:10.1175/JHM415.1.

Ellis, A. W. and D. J. Leathers, 1999: Analysis of cold airmass temperature modification across the US Great Plains as a consequence of snow depth and albedo. *Journal of Applied Meteorology and Climatology*, **38**, 696-711, doi:10.1175/1520-0450(1999)038<0696:AOCATM>2.0.CO;2.

Frei, A. and D. A. Robinson, 1999: Northern Hemisphere snow extent: regional variability 1972-1994. *International Journal of Climatology*, **19**(14), 1535-1560, doi:10.1002/(SICI)1097-0088(19991130)19:14<1535::AID-JOC438>3.0.CO;2-J.

Finnis, J. M. M. Holland, M. C. Serreze, and J. J. Cassano, 2007: Response of Northern Hemisphere extratropical cyclone activity and associated precipitation to climate change, as represented by the Community Climate System Model. *Journal of Geophysical Research: Biogeosciences*, **112**(G4), doi:10.1029/2006JG000286.

Folland, C. K., N. A. Rayner, S. J. Brown, T. M. Smith, S. S. P. Shen, D. E. Parker, I. Macadem, P. D. Jones, R. N. Jones, N. Nicholls, and D. M. H. Sexton, 2001: Global

temperature change and its uncertainties since 1861. *Geophysical Research Letters*, **28**(13), 2621-2624, doi:10.1029/2001GL012877.

Gan, T. Y., R. G. Barry, M. Gizaw, A. Gobena, and R. Balaji, 2013: Changes in North American snowpacks for 1979-2007 detected from the snow water equivalent data of SMMR and SSM/I passive microwave and related climatic factors. *Journal of Geophysical Research: Atmospheres*, **118**(14), 7682-7697, doi:10.1002/jgrd.50507.

Geng, Q. and M. Sugi, 2003: Possible change of extratropical cyclone activity due to enhanced greenhouse gases and sulfate aerosols – study with a high-resolution AGCM. *Journal of Climate*, **16**, 2262-2274, doi:10.1175/1520-0442(2003)16<2262:PCOECA>2.0.CO;2.

Golubev, V. N. and D. M. Frolov, 2015: Water vapor flows across snow-air and snow-soil interfaces. *Physicochemical Processes in Ice and Permafrost*, **19**(1), 20-26.

Grotjahn, R., 2015: Baroclinic Instability. In: *Encyclopedia of Atmospheric Sciences: Second Edition* [North, G. R., J. Pyle, and F. Zhang (eds.)] (pp. 304-312). Elsevier Inc., doi:10.1016/B978-0-12-382225-3.00076-1

Hansen, J., M. Sato, R. Ruedy, K. Lo, D. W. Lea, and M. Medina-Elizade, 2006: Global temperature change. *Proceedings of the National Academy of Sciences of the United States of America*, **103**(39), 14288-14293, doi:10.1073/pnas.0606291103.

Hawcroft, M. K., L. C. Shaffrey, K. I. Hodges, H. F. Dacre, 2012: How much Northern Hemisphere precipitation is associated with extratropical cyclones?. *Geophysical Research Letters*, **39**(24), doi:10.1029/2012GL053866.

Heim, R. and K. F. Dewey, 1984: Circulation patterns and temperature fields associated with extensive snow cover on the North American continent. *Physical Geography*, **5**(1), 66-85, doi:10.1080/02723646.1984.10642244.

Hong, S.-Y., J. Dudhia, S.-H. Chen, 2004: A revised approach to ice microphysical processes for the bulk parameterization of clouds and precipitation. *Monthly Weather Review*, **132**, 103-120, doi:10.1175/1520-0493(2004)132<0103:ARATIM>2.0.CO;2.

Inatsu, M., H. Mukougawa, and S. Xie, 2002: Tropical and extratropical SST effect on the midlatitude storm track. *Journal of the Meteorological Society of Japan*, **80**(4B), 1069-1076.

Jacoby, G. C. and R. D'Arrigo, 1989: Reconstructed Northern Hemisphere annual temperature since 1671 based on high-latitude tree-ring data from North America. *Climatic Change*, **14**(1), 39-59, doi:10.1007/BF00140174.

Jeong, J., H. W. Linderholm, S. Woo, C. Folland, B. Kim, S. Kim, and D. Chen, 2013: Impacts of snow initialization on subseasonal forecasts of surface air temperature for the cold season. *Journal of Climate*, **26**, 1956-1972, doi:10.1175/JCLI-D-12-00159.1.

Jones, P. D., 1988: Hemispheric surface air temperature variations: recent trends and an update to 1987. *Journal of Climate*, **1**, 654-660, doi:10.1175/1520-0442(1988)001<0654:HSATVR>2.0.CO;2

Kapnick, S. A. and T. L. Delworth, 2013: Controls of global snow under a changed climate. *Journal of Climate*, **26**, 5537-5562, doi:10.1175/JCLI-D-12-00528.1.

Kirchhoff, G., 1860: Ueber das Verhältniss zwischen dem Emissionsvermögen und dem Absorptionsvermögen der Körper für Wärme and Licht. *Annalen der Physik und Chemie*, **109**(2), 275-301, doi:10.1002/andp.18601850205. Translated by Guthrie, F. as G. Kirchoff, 1860: On the relation between the radiating and absorbing powers of different bodies for light and heat. *Philosophical Magazine, Series 4*, **20**, 1-21.

Kopp, T. J. and R. B. Kiess, 1996: The Air Force Global Weather Central Snow Analysis Model. *15th Conference on Weather Analysis and Forecasting*, American Meteorological Society, Norfolk, VA, 220-222.

Krasting, J. P., A. J. Broccoli, K. W. Dixon, and J. R. Lanzante, 2013: Future changes in North American snowfall. *Journal of Climate*, **26**, 7813-7828, doi:10.1175/JCLI-D-12-00832.1.

Kung, E. C., R. A. Bryson, and D. H. Lenschow, 1964: Study of a continental surface albedo on the basis of flight measurements and structure of the Earth's surface snow cover over North America. *Monthly Weather Review*, **92**(12), 543-564, doi:10.1175/1520-0493(1964)092<0543:SOACSA>2.3.CO;2.

Lamb, H. H., 1955: Two-way relationship between the snow or ice limit and the 1,000-500 mb thickness in the overlying atmosphere. *Quarterly Journal of the Royal Meteorological Society*, **81**(348), 172-189, doi:10.1002/qj.49708134805.

Leathers, D. J., A. W. Ellis, and D. A. Robinson, 1995: Characteristics of temperature depressions associated with snow cover across the Northeast United States. *Journal of Applied Meteorology and Climatology*, **34**, 381-390, doi:10.1175/1520-0450-34.2.381

Lemke, P., J. Ren, R. B. Alley, I. Allison, J. Carrasco, G. Flato, Y. Fujii, G. Kaser, P. Mote, R. H. Thomas, and T. Zhang, 2007: Observations: Changes in Snow, Ice, and Frozen Ground. In: *Climate Change 2007: The Physical Science Basis. Contribution of Working Group I to the Fourth Assessment Report of the Intergovernmental Panel on Climate Change* [Solomon, S., D. Qin, M. Manning, Z. Chen, M. Marquis, K. B. Averyt, M. Tignor, and H. L. Miller (eds.)]. Cambridge University Press, Cambridge, United Kingdom and New York, NY, USA.

Livneh, B., Y. Xia, K. E. Mitchell, M. B. Ek, and D. P. Lettenmaier, 2010: Noah LSM snow model diagnostics and enhancements. *Journal of Hydrometeorology*, **11**, 721-738, doi:10.1175/2009JHM1174.1

Ma, C. -G. and E. K. M. Chang, 2017: Impacts of storm-track variations of wintertime extreme weather events over the continental United States. *Journal of Climate*, **30**, 4601-4624, doi:10.1175/JCLI-D-16-0560.1.

Maloney, E. D., S. J. Camargo, E. Chang, B. Colle, R. Fu, K. L. Geil, Q. Hu, X. Jiang, N. Johnson, K. B. Karnauskas, J. Kinter, B. Kirtman, S. Kumar, B. Langenbrunner, K. Lombardo, L. N. Long, A. Mariotti, J. E. Meyerson, K. C. Mo, J. D. Neelin, Z. Pan, R. Seager, Y. Serra, A. Seth, J. Sheffield, J. Stroeve, J. Thibeault, S. Xie, C. Wang, B. Wyman, and M. Zhao, 2014: North American Climate in CMIP5 experiments: Part III: Assessment of twenty-first-century projections. *Journal of Climate*, **27**, 2230-2270, doi:10.1175/JCLI-D-13-00273.1.

Manabe, S. and R. T. Wetherald, 1980: On the distribution of climate change resulting from an increase in CO₂ content of the atmosphere. *Journal of Atmospheric Sciences*, **37**, 99-118, doi:10.1175/1520-0469(1980)037<0099:OTDOCC>2.0.CO;2.

Marshall, S. and R. J. Oglesby, 1994: An improved snow hydrology for GCMs. Part 1: snow cover fraction, albedo, grain size, and age. *Climate Dynamics*, **10**(1-2), 21-37, doi:10.1007/BF00210334.

Mesinger, F., G. DiMego, E. Kalnay, K. Mitchell, P. C. Shafran, W. Ebisuzaki, D. Jović, J. Woollen, E. Rogers, E. H. Berbery, M. B. Ek, Y. Fan, R. Grumbine, W. Higgins, H. Li, Y. Lin, G. Manikin, D. Parrish, and W. Shi, 2006: North American Regional Reanalysis. *Bulletin of the American Meteorological Society*, **87**(3), 343-360, doi:10.1175/BAMS-87-3-343.

Mitchell, K., M. Ek, V. Wong, D. Lohmann, V. Koren, J. Schaake, Q. Duan, G. Gayno, B. Moore, P. Grunmann, D. Tarpley, B. Ramsay, F. Chen, J. Kim, H.-L. Pan, Y. Lin, C. Marshall, L. Mahrt, T. Meyers, and P. Ruscher, 2005: The Community Noah Land Surface Model (LSM) User's Guide Public Release Version 2.7.1, doi:10.1.1.705.9364.

Namias, J., 1962: Influences of abnormal heat sources and sinks on atmospheric behavior. *Proceedings of the International Symposium on Numerical Weather Prediction*, Tokyo, Japan, Meteorological Society of Japan, 615-627.

Namias, J., 1985: Some empirical evidence for the influence of snow cover on temperature and precipitation. *Monthly Weather Review*, **113**, 1542-1553, doi:10.1175/1520-0493(1985)113<1542:SEEFTI>2.0.CO;2.

Notaro, M., V. Bennington, and S. Vavrus, 2015: Dynamically downscaled projections of lake-effect snow in the Great Lakes Basin. *Journal of Climate*, **28**, 1661-1684, doi:10.1175/JCLI-D-14-00467.1.

Peacock, S., 2012: Projected twenty-first-century changes in temperature, precipitation, and snow cover over North America in CCSM4. *Journal of Climate*, **25**, 4405-4429, doi:10.1175/JCLI-D-11-00214.1.

Persson, M., 1975: Water budget estimations in the Lapträsket basin. *Northern Research Basins Symposium*, Edefors Sweden, April 1975.

Petty, G. W., 2006: *A First Course in Atmospheric Radiation*. Sundog Publishing, Madison, WI, USA.

Plummer, D. A., 2006: Climate and climate change over North America as simulated by the Canadian RCM. *Journal of Climate*, **19**, 3112-3132, doi:10.1175/JCLI3769.1.

Qu, X. and A. Hall, 2007: What controls the strength of snow-albedo feedback?. *Journal of Climate*, **20**(15), 3971-3981, doi:10.1175/JCLI4186.1.

Räisänen, J., 2007: Warmer climate: less or more snow?. *Climate Dynamics*, **30**, 307-309, doi:10.1007/s00382-007-0289-y.

Rayner, N. A., D. E. Parker, E. B. Horton, C. K. Folland, L. V. Alexander, D. P. Rowell, E. C. Kent, and A. Kaplan, 2003: Global analyses of sea surface temperature, sea ice, and night marine air temperature since the late nineteenth century. *Journal of Geophysical Research: Atmospheres*, **108**(D14), doi:10.1029/2002JD002670.

Reitan, C. H., 1974: Frequencies of cyclones and cyclogenesis for North America, 1951-1970. *Monthly Weather Review*, **102**, 861-868, doi:10.1175/1520-0493(1974)102<0861:FOCACF>2.0.CO;2.

Rhoades, A. M., P. A. Ullrich, and C. M. Zarzycki, 2018: Projecting 21st century snowpack trends in western USA mountains using variable-resolution CESM. *Climate Dynamics*, **50**, 261-288, doi:10.1007/s00382-017-3606-0.

Robinson, D. A. and G. Kukla, 1985: Maximum surface albedo of seasonally snow-covered lands in the northern hemisphere. *Journal of Applied Meteorology and Climatology*, **24**, 402-411, doi:10.1175/1520-0450(1985)024<0402:MSAOSS>2.0.CO;2.

Robinson, D. A. and K. F. Dewey, 1990: Recent secular variations in the extent of Northern Hemisphere snow cover. *Geophysical Research Letters*, **17**(10), 1557-1560, doi:10.1029/GL017i010p01557.

Robinson, D. A. and M. G. Hughes, 1991: Snow cover variability on the northern and central Great Plains. *Great Plains Research*, **1**(1), 93-113.

Robinson, D. A., 1996: Evaluating snow cover over Northern Hemisphere lands using satellite and in situ observations. *Proceedings of the 53rd Eastern Snow Conference*, Williamsburg, VA, 13-19.

Robinson, D. A. and A. Frei, 2000: Seasonal variability of Northern Hemisphere snow extent using visible satellite data. *The Professional Geographer*, **52**(2), 307-315, doi:10.1111/0033-0124.

Roeckner, E., G. Bäuml, L. Bonaventura, R. Brokopf, M. Esch, M. Giorgetta, S. Hagemann, I. Kirchner, L. Kornbluh, E. Manzini, A. Rhodin, U. Schlese, U. Schulzweida, and A. Tompkins, 2003: The atmospheric general circulation model ECHAM5. Part I: Model description. Max Planck Institute for Meteorology Rep. 349, 127 pp.

Ross, B. and J. E. Walsh, 1986: Synoptic-scale influences of snow cover and sea ice. *Monthly Weather Review*, **114**, 1795-1810, doi:10.1175/1520-0493(1986)114<1795:SSIOSC>2.0.CO;2.

Rydzik, M. and A. R. Desai, 2014: Relationship between snow extent and midlatitude disturbance centers. *Journal of Climate*, **27**, 2971-2982, doi:10.1175/JCLI-D-12-00841.1.

Shukla, J., 1984: Predictability of Time Averages: Part II: The Influence of the Boundary Forcings. In: *Problems and Prospects in Long and Medium Range Weather Forecasting* [Burridge, D. M. and E. Källén (eds.)]. Topics in Atmospheric and Oceanic Sciences. Springer, Berlin, Heidelberg.

Skamarock, W. C., J. B. Klemp, J. Dudhia, D. O. Gill, D. M. Barker, M. G. Duda, X.-Y. Huang, W. Wang, and J. G. Powers, 2008: A description of the Advanced Research WRF version 3. *NCAR Tech. Note NCAR/TN-475+STR*, 113 pp.

Sobolowski, S., G. Gong, and M. Ting, 2010: Modeled climate state and dynamic response to anomalous North American snow cover. *Journal of Climate*, **23**, 785-799, doi:10.1175/2009JCLI3219.1.

Sutcliffe, R. C., 1947: A contribution to the problem of development. *Quarterly Journal of the Royal Meteorological Society*, **73**(317-318), 370-383, doi:10.1002/qj.49707331710.

Taylor, K. E., R. J. Stouffer, and G. A. Meehl, 2012: An overview of CMIP5 and the experimental design. *Bulletin of the American Meteorological Society*, **93**(3), 485-498, doi:10.1175/BAMS-D-11-00094.1.

Teng, H., W. M. Washington, and G. A. Meehl, 2007: Interannual variations and future changes of wintertime extratropical cyclone activity over North America in CCSM3. *Climate Dynamics*, **30**(7-8), 673-686, doi:10.1007/s00382-007-0314-1.

Thomas, B. C. and J. E. Martin, 2007: A synoptic climatology and composite analysis of the Alberta Clipper. *Weather and Forecasting*, **22**, 315-333, doi:10.1175/WAF982.1.

Tomasi, E., L. Giovannini, D. Zardi, and M. de Franceschi, 2017: Optimization of Noah and Noah_MP WRF land surface schemes in snow-melting conditions over complex terrain. *Monthly Weather Review*, **145**, 4727-4745, doi:10.1175/MWR-D-16-0408.1.

Trenberth, K. E., 1998: Atmospheric moisture residence times and cycling: implications for rainfall rates and climate change. *Climate Change*, **39**, 667-694, doi:10.1023/A:1005319109110.

Trenberth, K. E., J. T. Fasullo, and T. G. Shepherd, 2015: Attribution of climate extreme events. *Nature Climate Change*, **5**, 725-730, doi:10.1038/NCLIMATE2657.

van Vuuren, D. P., J. Edmonds, M. Kainuma, K. Riahi, A. Thompson, K. Hibbard, G. C. Hurtt, T. Kram, V. Krey, J. Lamarque, T. Masui, M. Meinshausen, N. Nakicenovic, S. J. Smith, and S. K. Rose, 2011: The representative concentration pathways: an overview. *Climatic Change*, **109**, 5-31, doi:10.1007/s10584-011-0148-z.

Vavrus, S., 2007: The role of terrestrial snow cover in the climate system. *Climate Dynamics*, **29**(1), 73-88, doi:10.1007/s00382-007-0226-0.

Wagner, J. A., 1973: The influence of average snow depth on the monthly mean temperature anomaly. *Monthly Weather Review*, **101**(8), 624-626, doi:10.1175/1520-0493(1973)101<0624:TIOASD>2.3.CO;2.

Walland and Simmonds, 1997: Modelled atmospheric response to changes in Northern Hemisphere snow cover. *Climate Dynamics*, **13**(1), 25-34, doi:10.1007/s003820050150.

Wallen, C. C., 1949: The shrinkage of the Kårsa Glacier and its probable meteorological causes. *Geografiska Annaler*, **31**(1-4), 275-291, doi:10.1080/20014422.1949.11880811.

Warren, S. G., 1984: Impurities in snow: effects on albedo and snowmelt (review). *Annals of Glaciology*, **5**, 177-179, doi:10.3189/1984AoG5-1-177-179.

West, A. J., and K. R. Knoerr, 1959: Water losses in the Sierra Nevada. *Journal of the American Water Works Association*, **51**(4), 481-488.

Wuebbles, D., G. Meehl, K. Hayhoe, T. R. Karl, K. Kunkel, B. Santer, M. Wehner, B. Colle, E. M. Fischer, R. Fu, A. Goodman, E. Janssen, V. Kharin, H. Lee, W. Li, L. N. Long, S. C. Olsen, Z. Pan, A. Seth, J. Sheffield, and L. Sun, 2014: CMIP5 climate model analyses: Climate extremes in the United States. *Bulletin of the American Meteorological Society*, **95**(4), 571-583, doi:10.1175/BAMS-D-12-00172.1.

Yin, J. H., 2005: A consistent poleward shift of the storm tracks in simulations of 21st century climate. *Geophysical Research Letters*, **32**(18), doi:10.1029/2005GL023684

Zhang, T., K. Stamnes, and S. A. Bowling, 1996: Impact of clouds on surface radiative fluxes and snowmelt in the Arctic and Subarctic. *Journal of Climate*, **9**, 2110-2123, doi:10.1175/1520-0442(1996)009<2110:IOCSR>2.0.CO;2.

Zhang, T., T. E. Osterkamp, and K. Stamnes, 1997: Effects of climate on the active layer and permafrost on the north slope of Alaska, USA. *Permafrost and Periglacial Processes*, **8**(1), 45-67, doi:10.1002/(SICI)1099-1530(199701)8:1<45::AID-PPP240>3.0.CO;2-K.

Zhang, T., 2005: Influence of the seasonal snow cover on the ground thermal regime: an overview. *Reviews of Geophysics*, **43**(4), doi:10.1029/2004RG000157.

Zishka, K. M. and P. J. Smith, 1980: The climatology of cyclones and anticyclones over North America and surrounding ocean environs for January and July, 1950-77. *Monthly Weather Review*, **108**(4), 387-401, doi:10.1175/1520-0493(1980)108<0387:TCOCAA>2.0.CO;2.

7 Figures and Tables

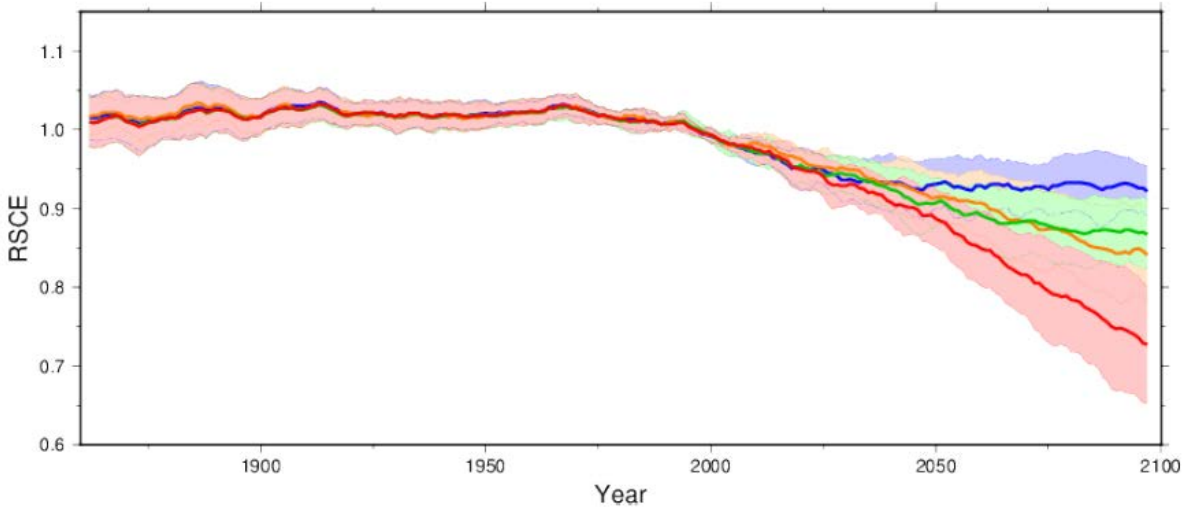


Figure 1. From Brutel-Vuilmet et al. (2013): Projected Northern Hemisphere March–April average seasonal snow cover extent (RSCE, relative to the 1986–2005 reference period) for the different RCP scenarios (blue: RCP2.6; green: RCP4.5; yellow: RCP6.0; red: RCP8.5), multi-model average over all available models for each scenario. The 5-yr running average ensemble mean is taken for each individual model before the multi-model average is calculated. Inter-model spread is represented as plus or minus one standard deviation from the multi-model mean.

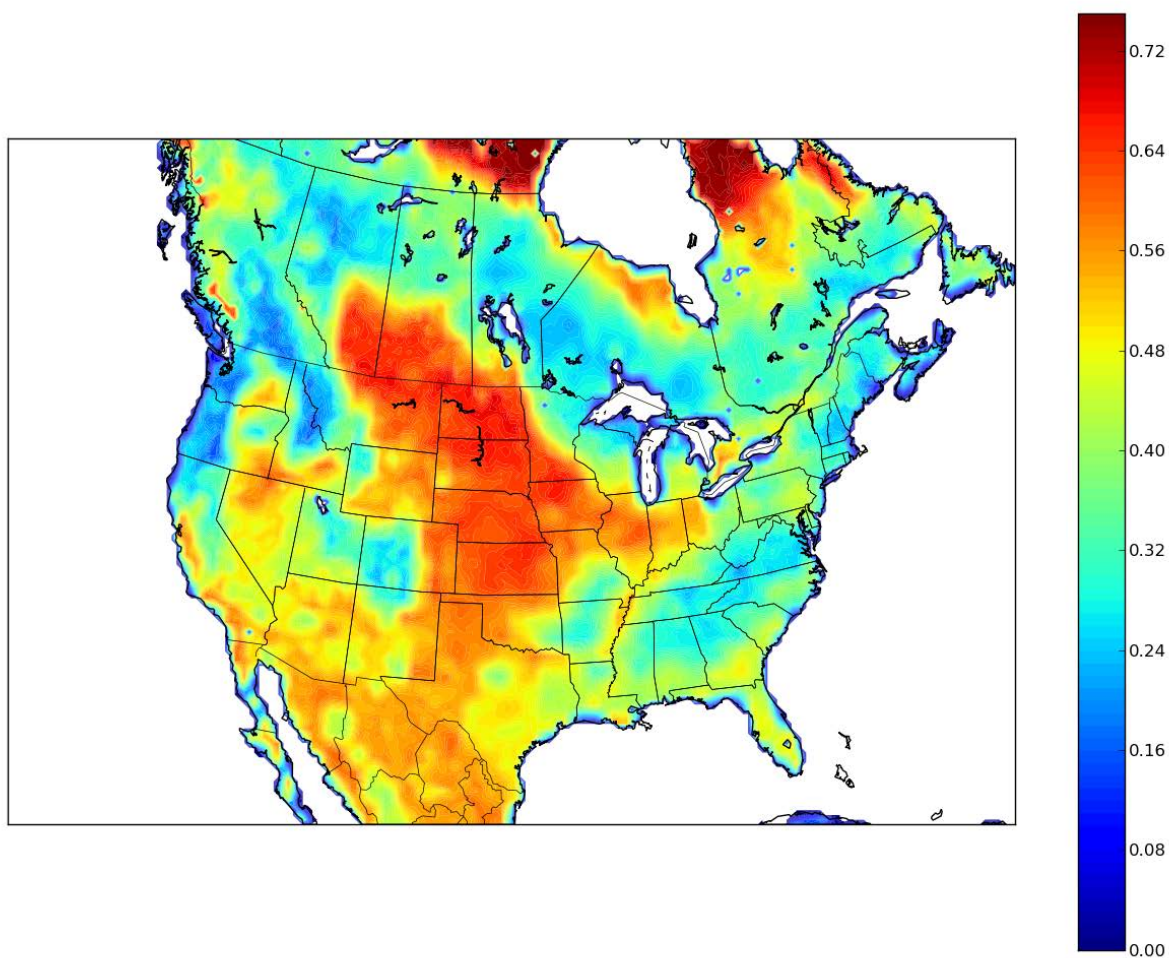


Figure 2. Difference between grid point maximum snow albedo (determined from Robinson and Kukla, 1985) and background surface albedo as established by the WRF Preprocessing System. The large region of maximum albedo difference in the center of the continent represents the Great Plains study area.

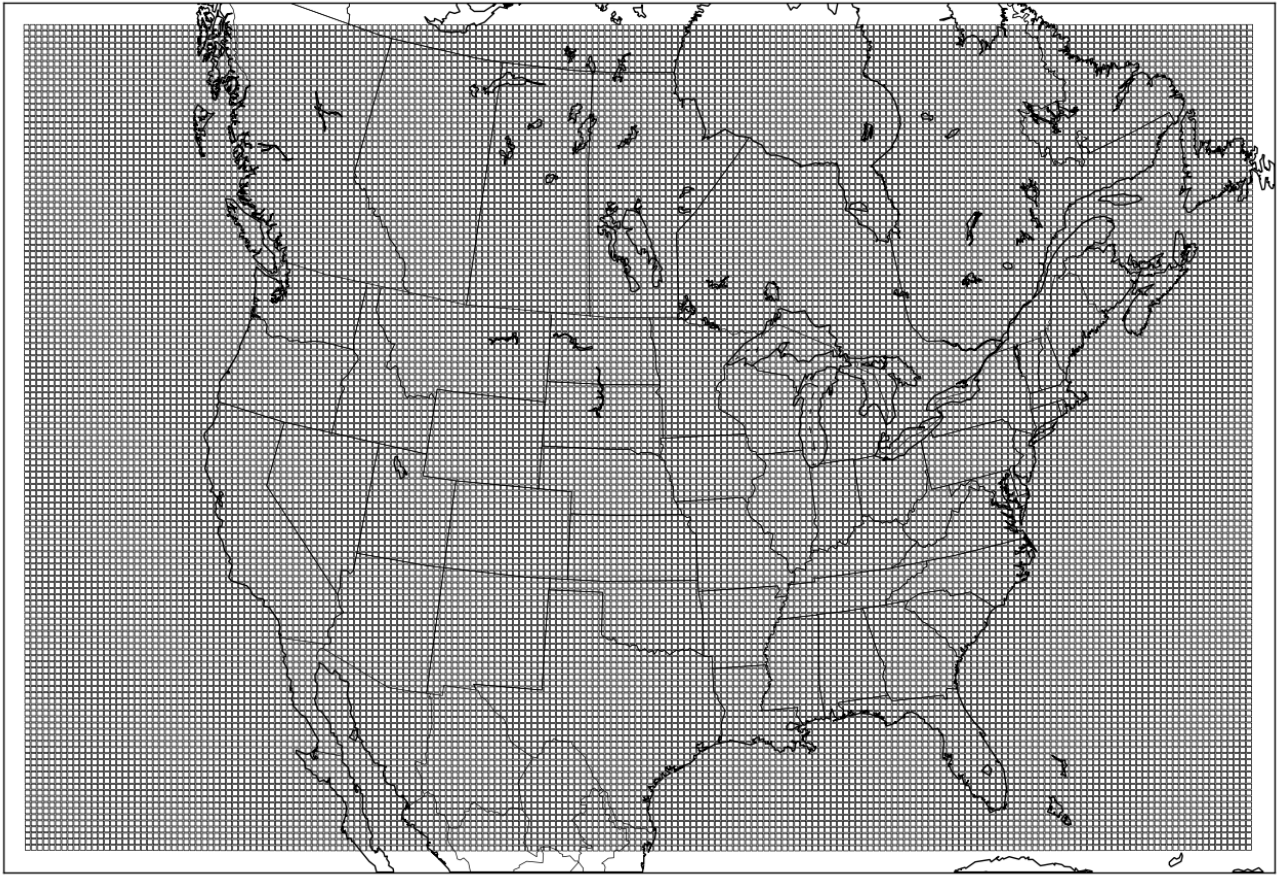


Figure 3. The domain utilized for WRF-ARW simulations. The 30 km grid spacing is shown with the black grid and the four grid cell buffer zone is left uncovered.

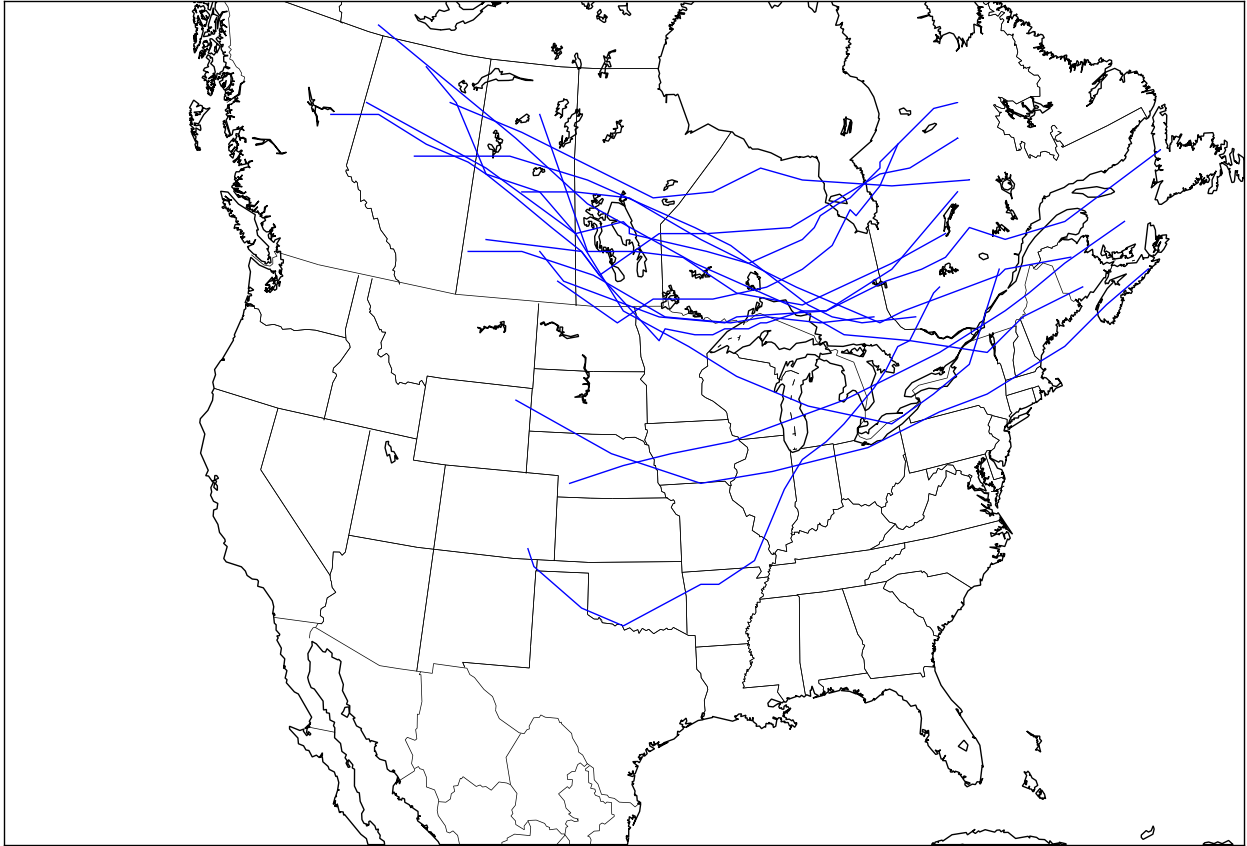


Figure 4. Cyclone trajectories for the 15 cases tested in this study.

Modeling Center (or Group)	Institute ID	Model Name	Horizontal Res. (°lon × °lat)	No. Vertical Levels
Commonwealth Scientific and Industrial Research Organization (CSIRO) and Bureau of Meteorology (BOM), Australia	CSIRO-BOM	ACCESS1.0	1.875 × 1.25	38
National Center for Atmospheric Research	NCAR	CCSM4	1.25 × 1.0	26
Centre National de Recherches Météorologique/Centre Européen de Recherche et Formation Avancée en Calcul Scientifique	CNRM-CERFACS	CNRM-CM5	1.4 × 1.4	31
Commonwealth Scientific and Industrial Research Organization in collaboration with Queensland Climate Change Centre of Excellence	CSIRO-QCCCE	CSIRO-Mk3.6.0	1.8 × 1.8	18
NASA Goddard Institute for Space Studies	NASA GISS	GISS-E2-H, GISS-E2-R	2.5 × 2.0	40
Met Office Hadley Centre	MOHC	HadGEM2-CC, HadGEM2-ES	1.8 × 1.25	60
Institute for Numerical Mathematics	INM	INM-CM4	2.0 × 1.5	21
Atmosphere and Ocean Research Institute (The University of Tokyo), National Institute for Environmental Studies, and Japan Agency for Marine-Earth Science and Technology	MIROC	MIROC5	1.4 × 1.4	40
Max Planck Institute for Meteorology	MPI-M	MPI-ESM-LR	1.9 × 1.9	47
Meteorological Research Institute	MRI	MRI-CGCM3	1.1 × 1.1	48
Norwegian Climate Centre	NCC	NorESM1-M, NorESM1-ME	2.5 × 1.9	26

Table 1. CMIP5 models used in this study and their attributes

(see <http://cmip-pcmdi.llnl.gov/cmip5/>).

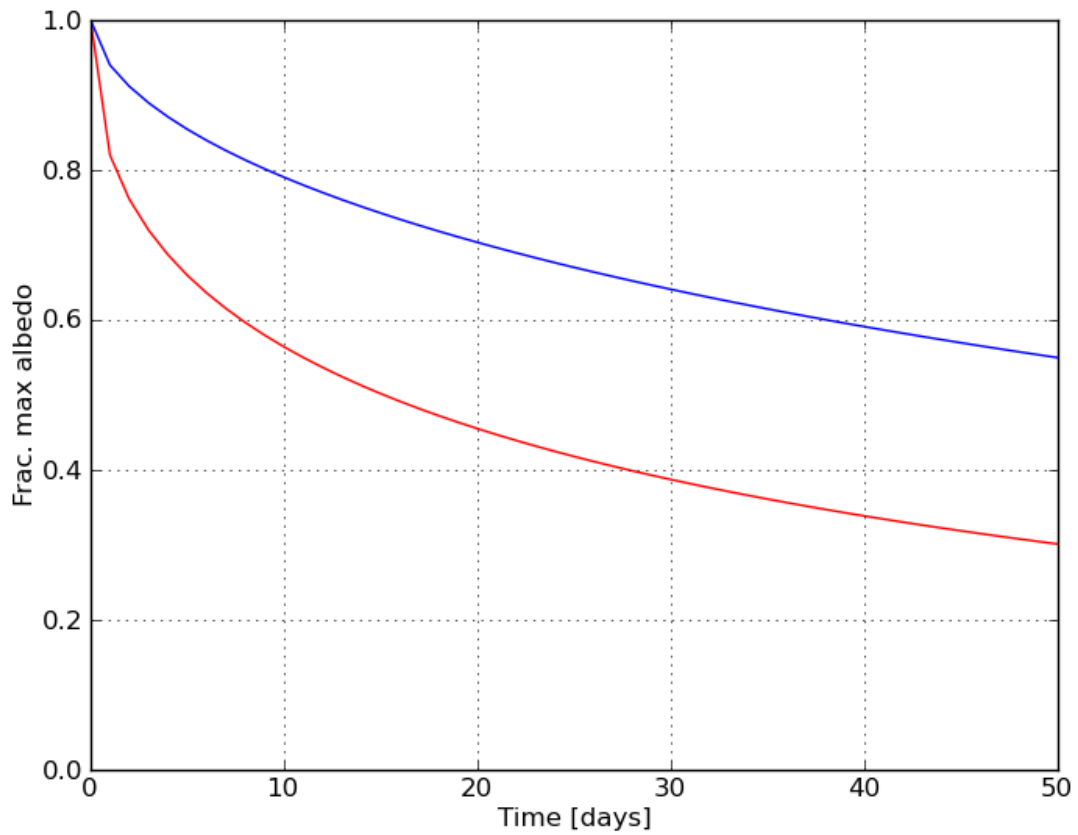


Figure 5. The fraction of maximum snow albedo which incident snow albedo is equal to according to its age in days as set forth by the equation from Livneh et al. (2010). The blue curve corresponds to accumulating snow fields while the red curve corresponds to ablating snow fields.

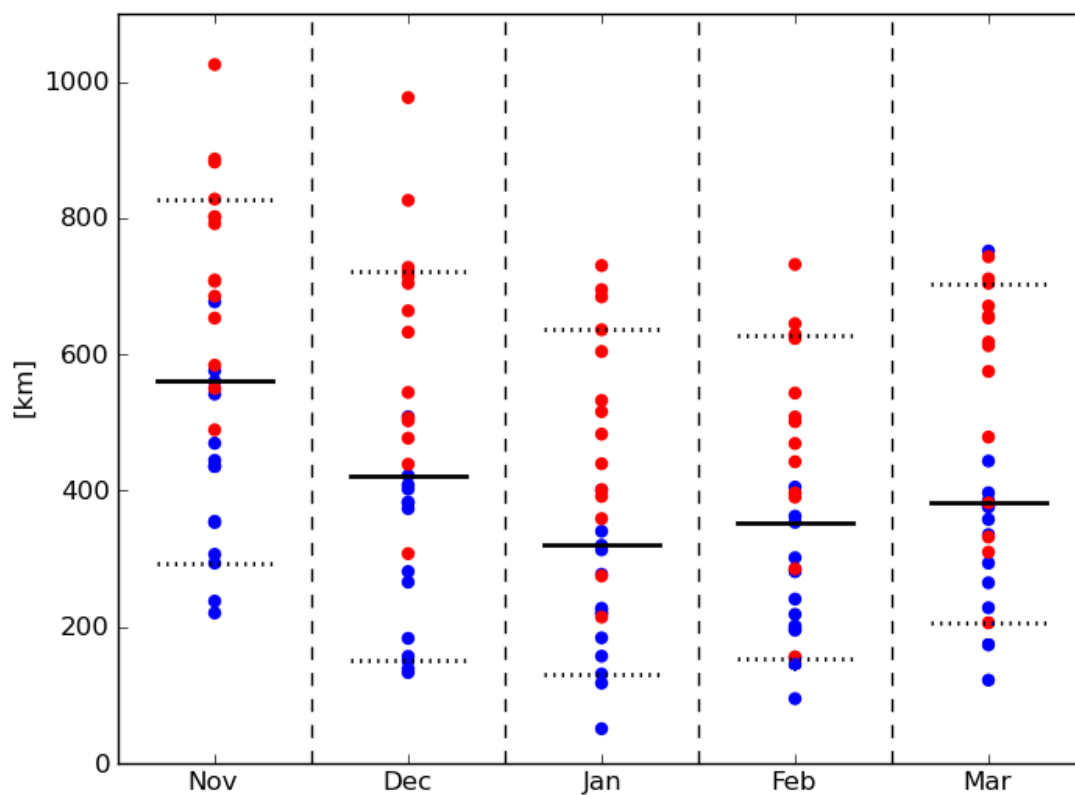


Figure 6. The distributions of average late twentieth to late twenty-first century snow extent retreat for each month as determined by 14 CMIP5 models. Values for RCP4.5 experiment are plotted in blue and RCP8.5 values are shown in red. Solid black horizontal bars indicate the median value while dotted bars indicate the tenth and ninetieth percentile values.

Month	10%	50%	90%
Nov	GISS-E2-R, RCP4.5	CNRM-CM5, RCP4.5	ACCESS1.0, RCP8.5
Dec	INM-CM4, RCP4.5	HadGEM2-ES, RCP4.5	CSIRO-Mk3.6.0, RCP8.5
Jan	GISS-E2-R, RCP4.5	MIROC5, RCP4.5	MIROC5, RCP8.5
Feb	MRI-CGCM3, RCP8.5	ACCESS1.0, RCP4.5	ACCESS1.0, RCP8.5
Mar	MRI-CGCM3, RCP8.5	CNRM-CM5, RCP8.5	MIROC5, RCP8.5

Table 2. Models and RCP experiments which were used for tenth, fiftieth, and ninetieth percentile perturbations for snow adjustment.

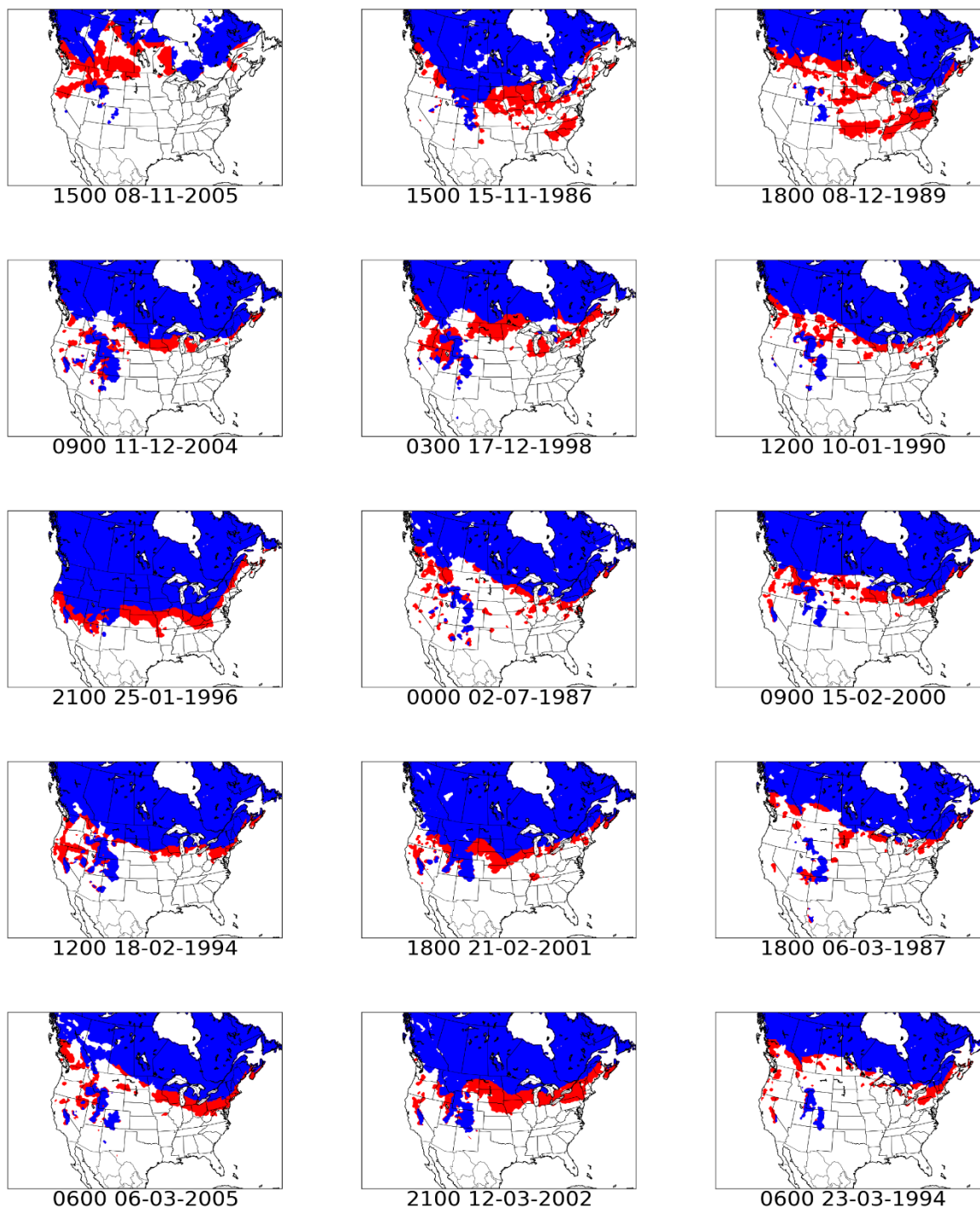


Figure 7. Observed snow extents (red) for each of the 15 cases modelled in this study and the perturbed snow extents (blue) created by application of the tenth percentile snow retreat values for the given month. Snow extents shown are represented as values of snow water equivalent above 1 kg m^{-2} .

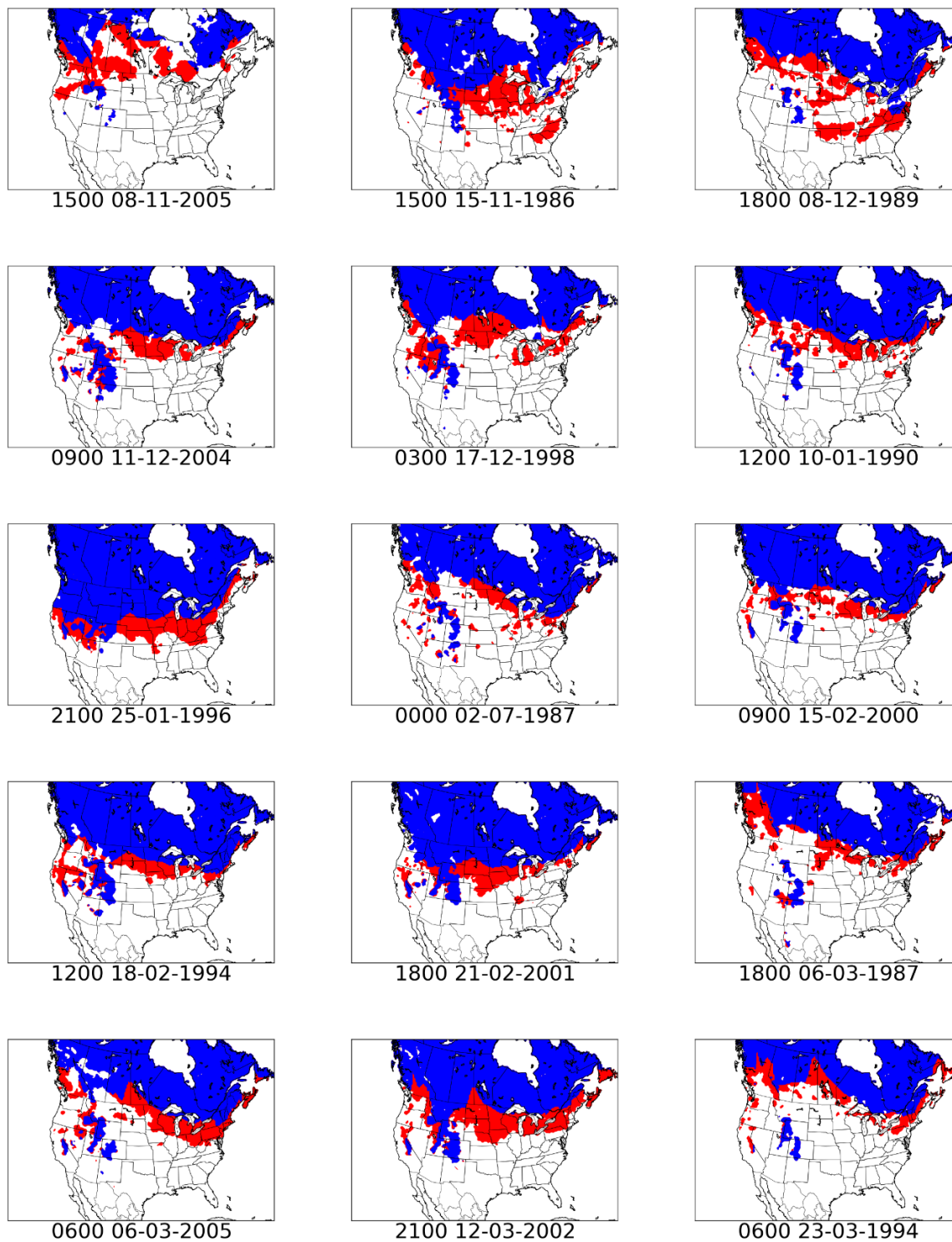


Figure 8. As for Figure 7 but for median snow retreat values.

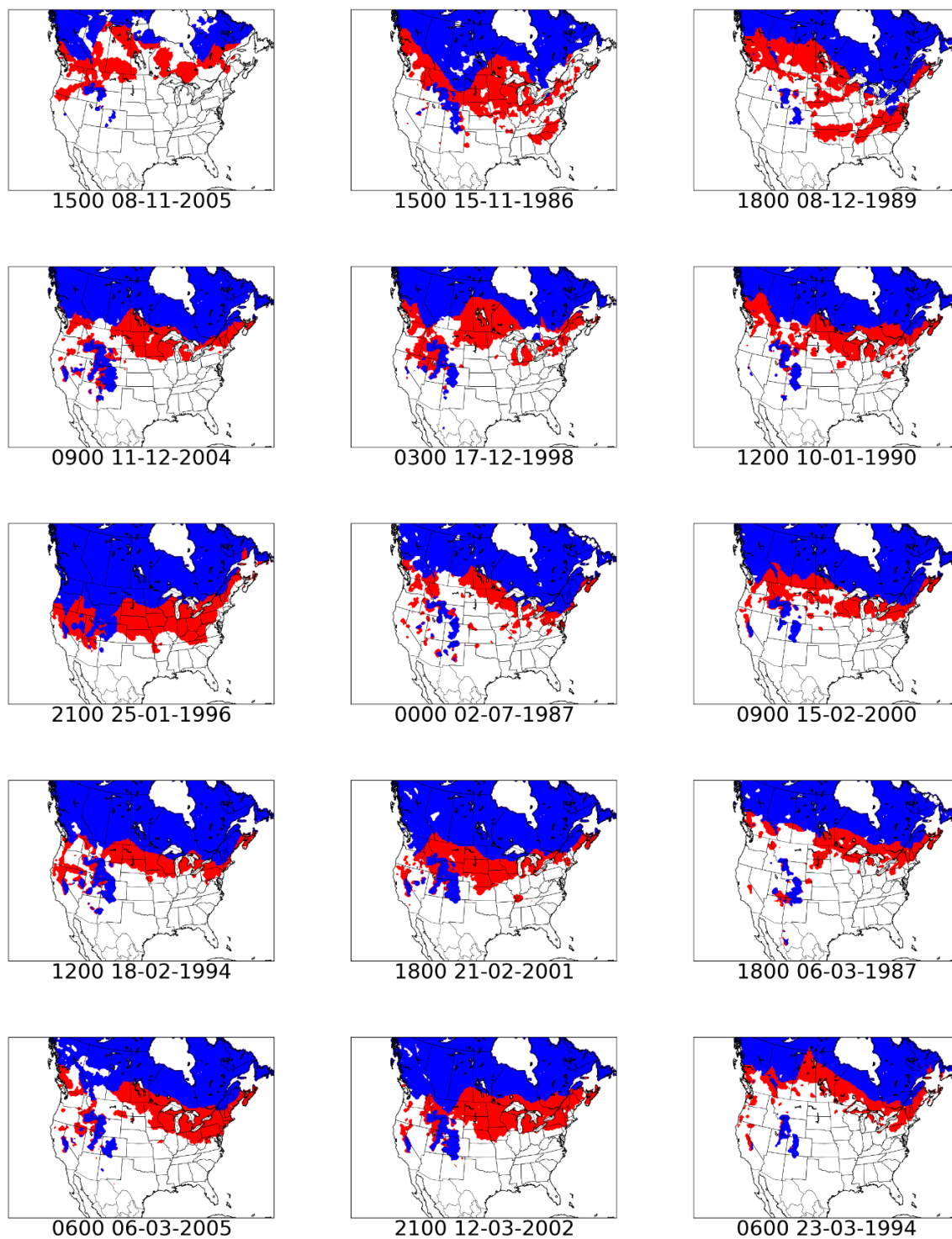


Figure 9. As for Figures 7 and 8 but for ninetieth percentile snow retreat values.

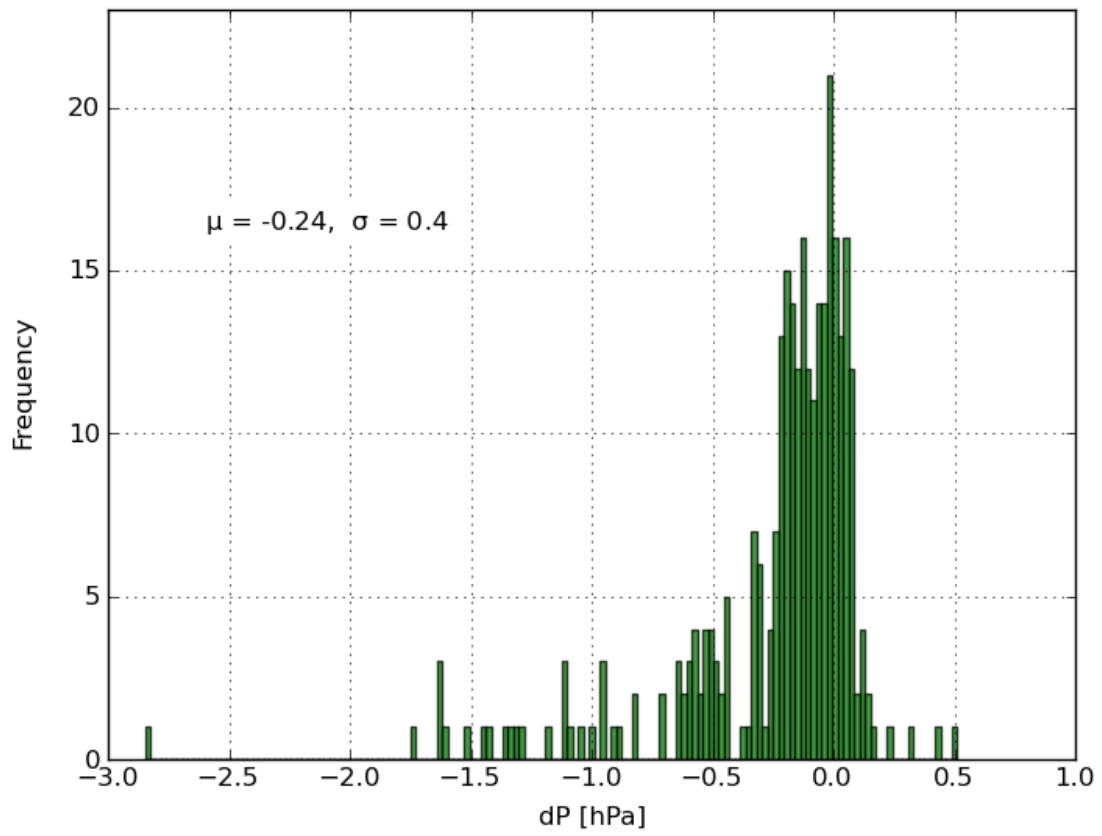


Figure 10. Histogram of mean change in pressure (hPa) averaged over the cyclone's lifetime for all simulations.

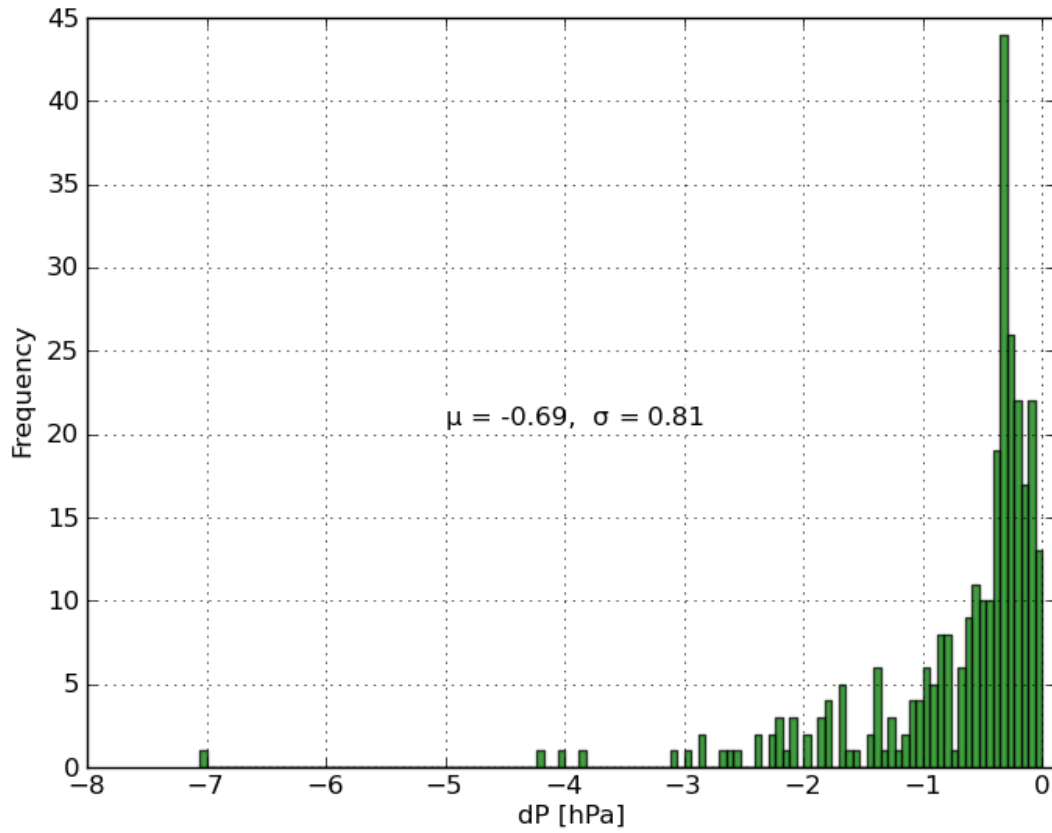


Figure 11. Histogram of maximum magnitude of pressure decrease (hPa) during the cyclone's lifetime for all simulations.

Adjustment	T-0	T-1	T-2	T-3	T-4
No snow	67%	80%	80%	87%	100%
Ninetieth	53%	73%	80%	93%	93%
Median	47%	80%	87%	87%	73%
Tenth	60%	73%	67%	80%	80%

Table 3. The percent of simulations which yielded an average decrease in central pressure during the lifetime of the cyclone categorized by each initialization time (T-*n* days prior to cyclogenesis) and snow extent perturbation. Color is used to emphasize percent values.

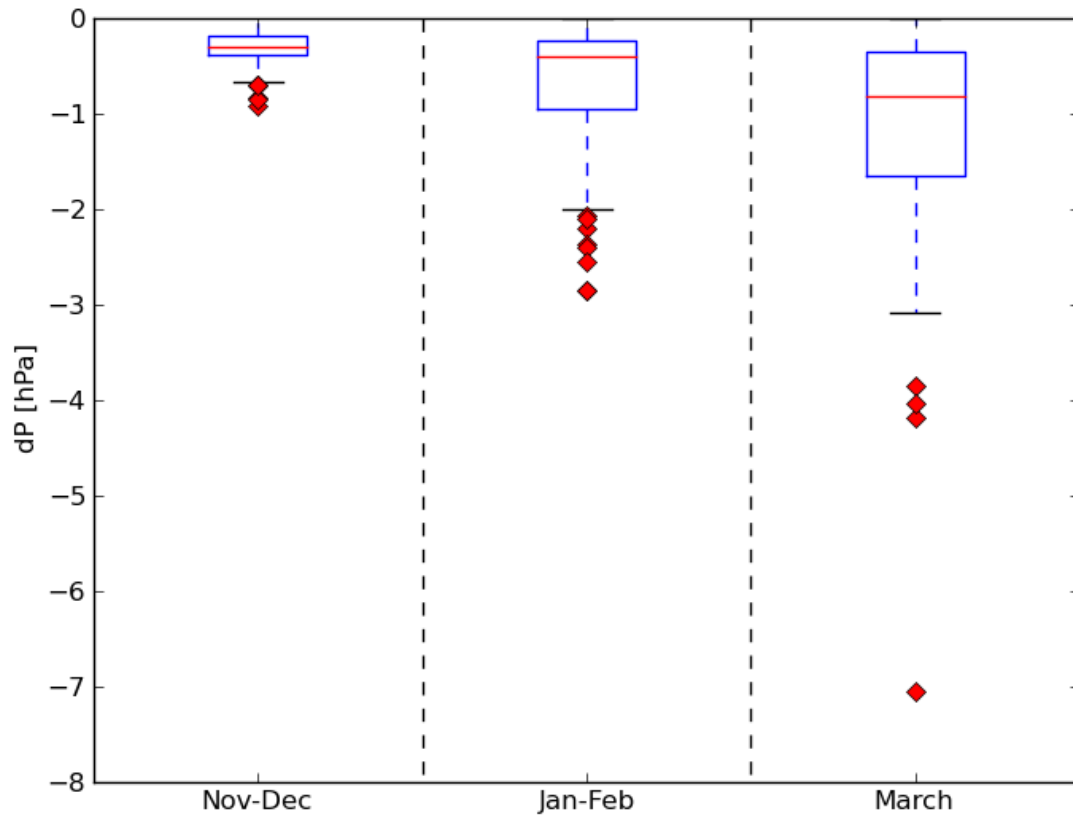


Figure 12. Maximum pressure decrease (hPa) across all simulations for the periods of November-December (N=100), January-February (N=120), and March (N=80).

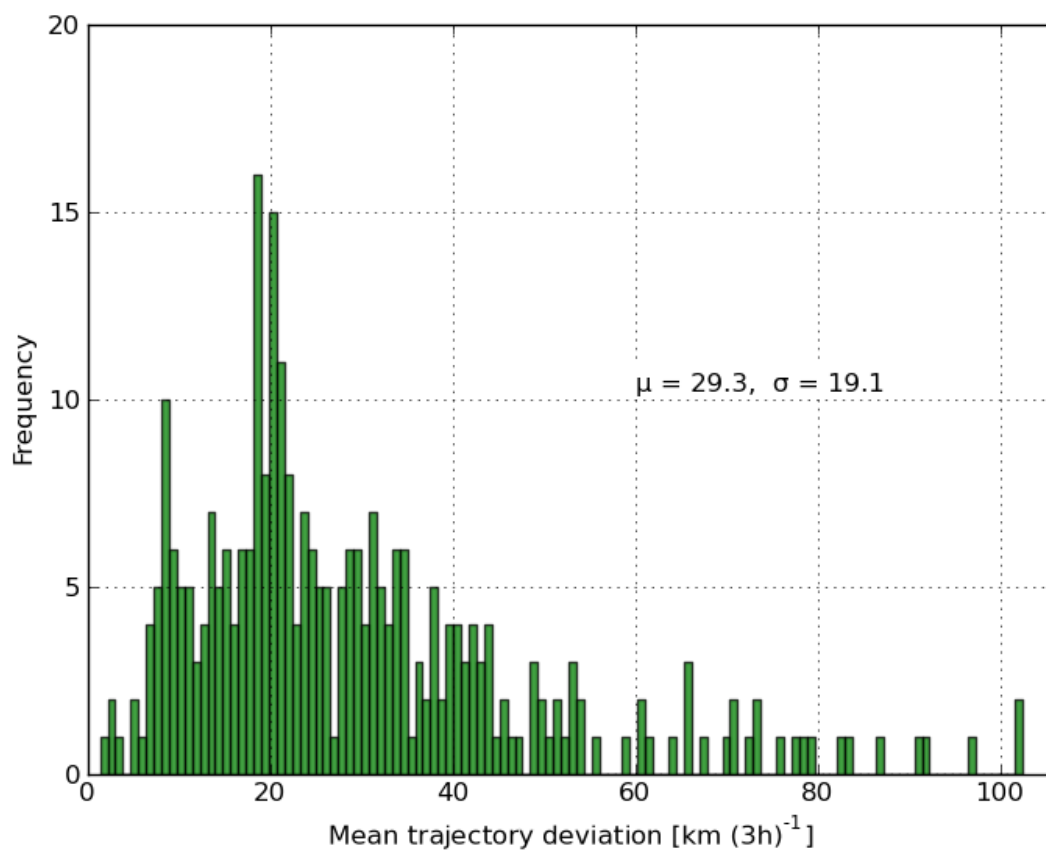


Figure 13. Histogram of mean trajectory deviation [km (3h)⁻¹] over the course of the cyclone's lifetime for all simulations.

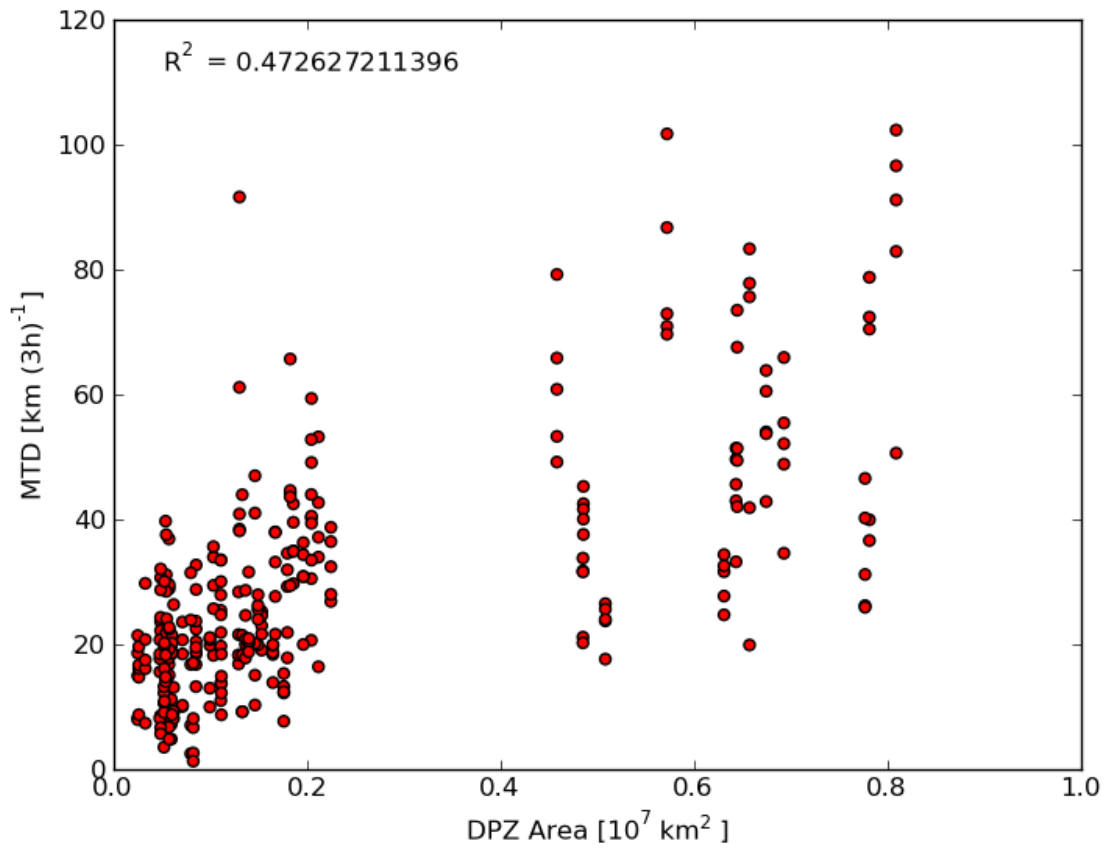


Figure 14. Mean trajectory deviation [km (3h)⁻¹] of all simulations plotted against the size of the depopulated zone (or total areal amount of snow removed for the perturbed simulation) for the corresponding simulation.

Adjustment	T-0	T-1	T-2	T-3	T-4
No snow	38.9	44.7	53.2	52	54.9
Ninetieth	23.8	27.4	31.9	30.2	35.1
Median	18.8	20.2	23.3	23.2	27.4
Tenth	14.2	13.3	17.4	18.1	17.9

Table 4. Average MTD in km (3h)^{-1} across all cases categorized by initialization time and applied snow retreat values. As for Table 3, color corresponds to the value of averaged MTD.

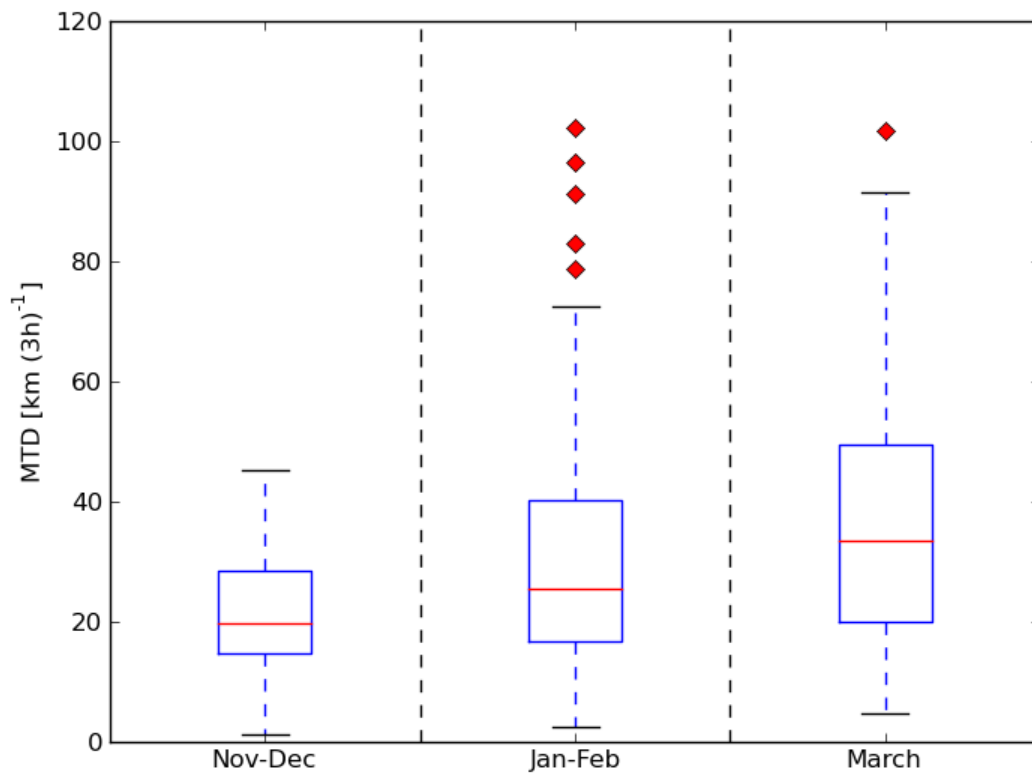


Figure 15. Mean trajectory deviation [km (3h)^{-1}] across all simulations for the periods of November-December (N=100), January-February (N=120), and March (N=80).

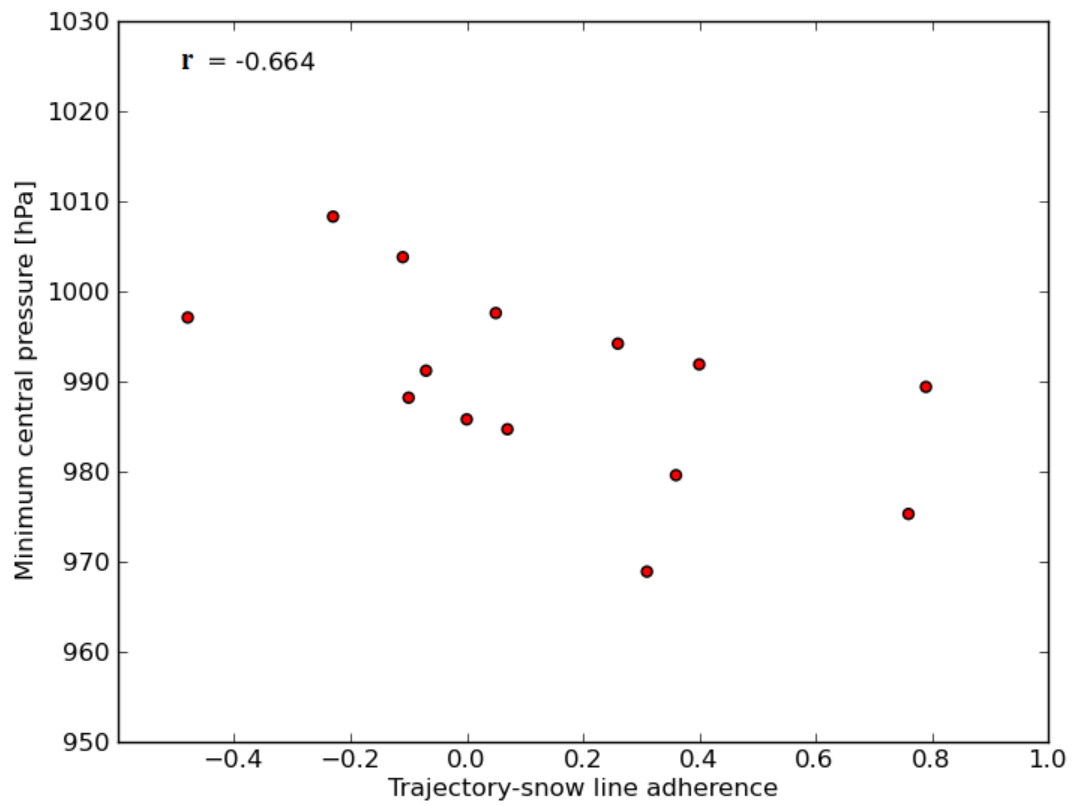


Figure 16. Relationship between observed minimum central pressure (hPa) of a cyclone and its adherence to the snow line.

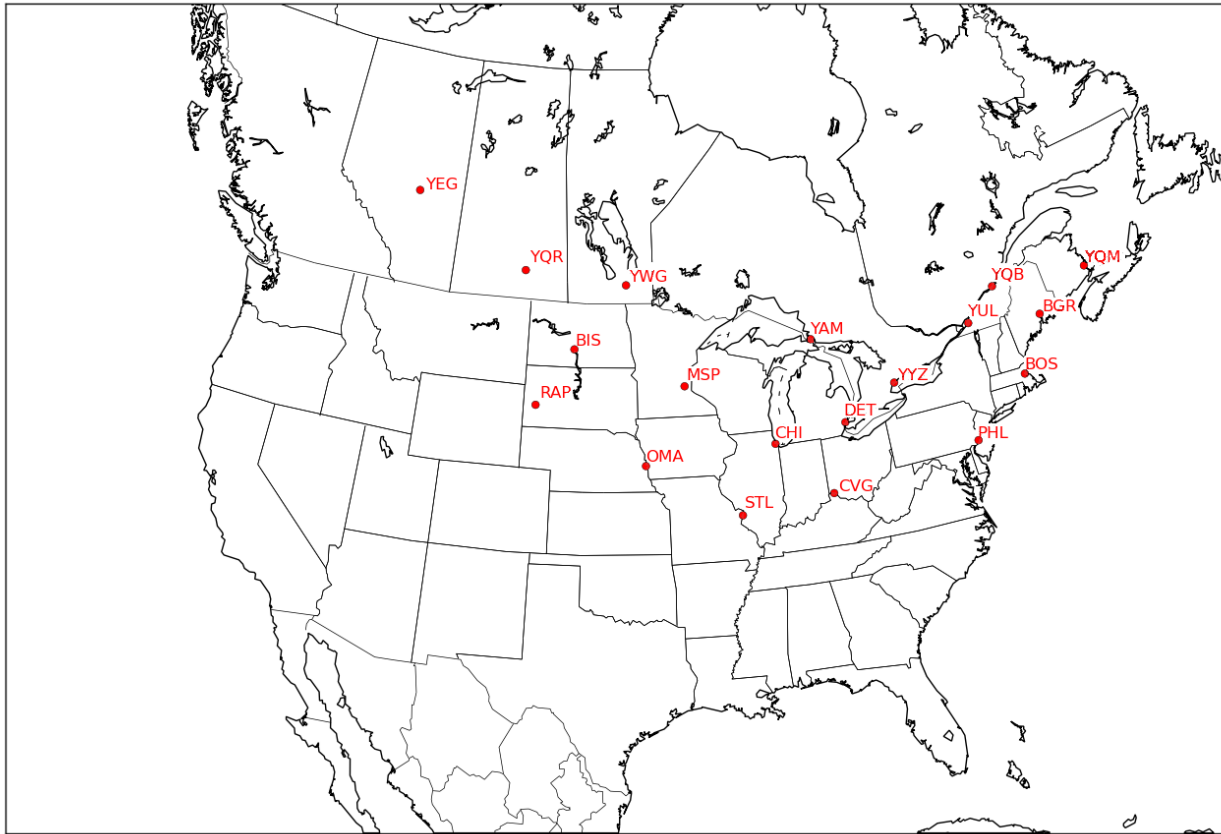


Figure 17. The 19 cities selected for examination in this study (airport codes given).

	Tenth			Median			Ninetieth		
	dMean	dMax	dMin	dMean	dMax	dMin	dMean	dMax	dMin
STL	0.3	0.2	0.6	0.5	0.4	0.9	0.8	0.7	1.3
CVG	0.3	0.1	0.4	0.4	0.1	0.6	0.4	0.3	0.7
OMA	0.3	0.2	0.3	0.9	0.6	1	1.5	0.9	1.9
PHL	0.5	0.6	0.6	0.5	0.6	0.6	0.8	0.7	1.2
CHI	0.4	0.4	0.4	0.6	0.5	0.5	0.8	0.6	0.8
DET	0.4	0.7	0.3	0.6	0.9	0.4	0.7	0.9	0.5
RAP	0	0.1	0	0.4	0.5	0.6	0.7	0.7	0.8
BOS	0.7	0.9	0.8	0.5	0.8	0.5	1.1	1	1.5
YYZ	0.2	0.2	0.2	0.4	0.2	0.5	0.9	0.5	1.4
MSP	0.7	0.6	0.5	2.2	1.4	2.5	5.1	3.9	6.4
BIS	0.2	0	0.2	0.5	0.3	0.4	2	1.8	2.2
YAM	0	0.2	0	0.2	0.3	0.4	1.1	0.6	2.7
YUL	0.1	0.2	0.1	0.5	0.3	0.3	1.4	0.4	1.6
BGR	0.2	0	0.1	0.3	0.1	0.3	1.1	0.2	1.4
YQB	0.1	0.1	0.1	0.3	0.1	0.1	0.7	0.3	0.7
YQM	1.2	0.1	2.3	1.3	0.2	2.3	1.7	0.4	2.8
YWG	0.1	0	0.4	1	0.8	1.4	1.6	0.9	2.8
YQR	0	0	0	1.2	0.6	1.6	1.6	1	2.1
YEG	0	0	0	0	0	0	0	0	0
Average	0.3	0.24211	0.38421	0.64737	0.45789	0.78421	1.26316	0.83158	1.72632

Table 5. The changes in mean, maximum, and minimum temperature for each city for the separate values of snow retreat for the months of January and February. Cities are arranged south to north by latitude from St. Louis at the top to Edmonton at the bottom.